Low-complexity echo cancellers for DMT-based asymmetric DSL transceivers

Jean-François Marceau

Department of Electrical & Computer Engineering
McGill University
Montreal, Canada

July 2005

2005/07/21

Canada

Abstract

In the past years, a number of researchers have investigated the use of digital echo cancellation systems for transmission technologies based on discrete multi-tone (DMT) modulation, such as that used in asymmetrical digital subscriber lines (ADSL) and the likes. Almost all the existing papers report on equal transmission rate systems, while little attention has been given to the multi-rate case. In fact, the first multi-rate echo canceller structure was developed by Ho *et al.*, and has always been referred since.

In this thesis, two sets of simplified techniques are developed. The first one reports on a fast initialization technique of the echo canceller. The method consists of replacing the first least mean square (LMS) iteration of the echo channel estimate by the solution of a system cost function in which circular convolution is assumed. The simplification of the method resides in the fact that no known sequence is used, and thus, no protocol is required.

The second simplified technique developed aims to reduce the computational complexity of the multi-rate echo canceller structure at the lower transmit rate side of the link, e.g. the line terminal side in ADSL. In this case, the echo canceller located in the terminal, processes the signals in the entire frequency bandwidth (higher rate). During the processing, the echo channel that is estimated corresponds in fact to the imperfect hybrid channel combined with the lowpass filtering action of the digital-to-analog converter (DAC) and the time-domain equalizer(TEQ). In such a situation, the frequency taps representing the estimated echo channel decay rapidly above the cutoff frequency of the DAC filter. In this work, we exploit this specific structure of the echo channel to reduce the computational complexity of the echo cancellation processing by setting a portion of the high frequency echo tap coefficients to zero, and by exploiting certain properties of the inverse Fast Fourier Transform (IFFT) algorithm.

Experimental simulations for an ADSL-like configuration involving 32 tones on the upstream and 256 tones on the downstream, showed that by employing the new proposed approach, the computational complexity can be reduced by a factor of as much as 53% while at the same time improving the achievable bitrate by 35 kbps. Furthermore, in regards of the initialization technique, the echo channel estimate convergence can be reached after around 6 iterations as compared to 15 for usual LMS algorithm.

Sommaire

Au cours des dernières années, plusieurs études ont été réalisées quant à la possibilité d'utiliser un système d'annulation d'écho dans les technologies de communications numériques basées sur la modulation à multitonalité discrète, tel que dans les lignes d'abonnés numériques à débit asymétrique (ADSL). La première structure d'annulation d'écho pour débit asymétrique a été développée par Ho *et al.*, et a toujours été référée par la suite.

Dans ce mémoire, des simplifications ont été apportées à deux types de techniques utilisées lors d'annulation d'écho. La première simplification a trait à l'initialisation du correcteur d'écho. La méthode consiste à remplacer la première itération du correcteur d'écho utilisant la méthode des moindres carrés moyens, par une solution minimisant une fonction de coût qui suppose que les convolutions réalisées dans le système sont circulaires. La simplification de la méthode réside dans le fait qu'aucune séquence connue de bits n'est utilisée et donc, qu'aucun protocole n'est requis.

La second groupe de techniques développées a pour but de réduire le nombre d'opérations arithmétiques dans la structure du correcteur d'écho à débit asymétrique qui est situé du coté de transmission qui transmet à faible débit, par exemple le terminal de la ligne en ADSL. Dans ce cas particulier, le correcteur d'écho situé dans le terminal traite les signaux électriques à haute fréquence. Lors du traitement des signaux, le canal d'écho estimé correspond à la combinaison des canaux de la jonction hybride, de l'égalisateur dans le domaine du temps et du filtre passe-bas présent dans le convertisseur numérique-analogique (DAC). La grandeur des coefficients représentant le canal d'écho estimé dans le domaine des fréquences se trouve donc à diminuer rapidement à partir du point de coupure du filtre passe-bas présent dans le DAC. Dans cet ouvrage, nous exploitons cette particularité du canal d'écho afin de réduire le nombre d'opérations arithmétiques en assignant la valeur des coefficients du canal correspondant aux hautes fréquences à zéro, et aussi, en exploitant certaines propriétés de la transformé inverse de Fourier (IFFT).

Des simulations expérimentales pour une configuration semblable à celle présente en ADSL impliquant 32 porteuses d'un coté et 256 de l'autre, ont démontré qu'en employant cette nouvelle approche, la complexité numérique pouvait être réduite de 53% tout en améliorant le taux de transmission de 35 kbps. En ce qui a trait à la technique d'initialisation du correcteur d'écho, les estimés du canal d'écho convergent après seulement environ 6 itérations comparativement à 15 sans l'utilisation de la méthode.

Acknowledgments

Contents

List of Figures

Chapter 1

Introduction

Digital Subscriber Line technology, better known as DSL, refers to the large family of digital communication technologies using traditional telephone lines as the physical medium to carry data. Since the early 1990s, DSL has gained more and more in popularity to become now one of the most widely used internet access technologies worldwide. The DSL family comprises: HDSL (High data rate DSL), SDSL (symmetric DSL), SHDSL, ADSL (asymmetric DSL), VHDSL (very high bit rate DSL) and more.

A telephone line is characterized by the copper twisted-wire-pair that links the customer's house to the central office. While the advantage of the DSL lies in the fact that every user has a dedicated link, one inconvenience is that the data transmitted to and from the customer is conveyed through the same unshielded wire. The separation of the upstream and downstream signals (coupling) is usually performed by a hardware circuit called a hybrid. Unfortunately, during the separation of the receive and transmit signals, the hybrid introduces interference in the received signal. This interference is called "echo" because it consists of (several) replications of the transmit signal at much lower levels (-40 dB and below). In the case where the transmit signal and receive signal occupy different frequency bands, the echo interference has little significance even though echo interference leakage exists. However, in the case where there is an overlap in the frequency bands occupied by the transmit and receive signals, for instance the echo cancelling mode in ADSL, the echo interference becomes much more significant and has to be removed through a digital signal processing algorithm called an echo canceller (EC).

Several aspects need to be taken into account when designing a DSL echo canceller.

The transmission/modulation scheme has to be considered in the first place. In fact, most of DSL technologies use discrete multi-tone (DMT) modulation. DMT requires the use of cyclic prefix, and sometimes cyclic suffix in the composition of the transmit signals. It also implies Fast Fourier Transform (FFT) of the signals. These particularities have already been very well exploited in the existing echo cancellers developed in the literature. Another characteristic that needs to be taken into account is that the a priori unknown echo channel varies according to the line impedance variations. Therefore, an echo canceller has to be adaptive in time. Finally, with the recent evolution of the DSL technologies, the frequency bandwidth employed has enlarged considerably which translates into more operations to be performed per unit of time. It follows that the number of computational operations required is another important criterion involved in EC design.

Consequently, EC can be enhanced by either increasing the convergence speed of the adaptive algorithm and/or by reducing the computational complexity. In this thesis, these two aspects will be addressed separately.

1.1 Literature survey

A number of echo canceller structures for DMT have been studied in the literature [1-7]. Each of them can be separated into two parts: adaptation and emulation. The adaptation corresponds to the part where the echo channel estimate is adapted, while the emulation corresponds to the part where the echo interference signal is recreated and subtracted from the receive signal. Echo canceller structures differ in the way the adaptation and emulation are realized.

Basic echo cancellation used to be completely realized in time domain. Cioffi et al. [1] were one of the first to investigate specific echo cancellation for discrete multi-tone (DMT) modulation. The innovation brought by [1] consisted of executing the adaptation in the frequency domain in such a manner that it reduces computational complexity. Later on, Ho et al. [2] exploited completely the frequency-domain idea previously introduced and elaborated an EC that performs the emulation mostly in the frequency domain. Thus, the only time-domain processing left was to make the recreated echo signal appear periodic. This set of time-domain operations is referred to as cyclic echo synthesizer (CES). In terms of complexity and notwithstanding the frame alignment, the structure proposed by [2] was very optimized.

The venue of the CES led Jones *et al.* [3] to investigate the optimal frame alignment between the receive and transmit signals. Indeed, by choosing a specific frame alignment, the number of operations to be processed in the CES can be reduced by half when compared with the zero frame alignment of [2].

Given that only one of the two terminal sides can optimize its timing alignment, Ysebaert *et al.* [6] took advantage of the frame alignment of [3] and created a new echo canceller structure for each terminal side. At the unaligned terminal side, the useful FFT block of the received far-end signal is thus aligned with the samples of the near-end signal that belong to two different frames. As a result the frequency-domain representation of the near-end signal is not available. To counter this problem, an extra FFT is applied on the proper near-end signal samples. This solution happens to be much simpler than the extra IFFT/FFT pair of the far-end received signal previously required in [2,4].

While the reduction of complexity was evolving, convergence speed was also improving. Indeed, [4–6] all included double talk cancellation in their echo canceller structure. The latter consists of removing the reconstructed far-end signal from the error signal before accomplishing the adaptation processing. In comparison with [2], convergence can be reached with 75% fewer iterations [4].

In regards of multi-rate communication, Ho *et al.* [2] were the first to propose specific echo canceller structures that take this case into account. Indeed, a multi-rate system means that one modem side has a transmit bandwidth smaller than its receive bandwidth whereas the modem on the other side has its transmit bandwidth larger than its receive bandwidth, thus the necessity of having two different EC structures. On the lower transmit bandwidth side, the strategy is to consider the transmit signal as if it was interpolated. In other words, the signal is represented in time-domain by inserting zeros between successive samples, and in frequency-domain by replicating the frequency response of the transmit signal. The number of successive zeros to be inserted and the number of replications of the frequency-domain response depend of the ratio between the transmit and receive bandwidths. The meaning of such doing is that the echo channel estimate includes the lowpass filtering action of the digital-to-analog converter (DAC).

Similarly, on the larger transmit bandwidth side, the strategy of the EC is to perform echo cancellation over the large frequency bandwidth by considering the interpolated version of the low bandwidth receive signal. More precisely, the interpolation of the received signal is performed by replicating the frequency error signal a certain number of times so

that it matches the large frequency bandwidth [2]. By doing so, it is possible to recreate an echo signal over the entire larger bandwidth. However since the received signal spreads over the lower bandwidth, the subtraction of the recreated echo signal from the received signal necessitates special operations in frequency and time domains. In frequency-domain, the recreated echo signal is first aliased in frequency before being subtracted from the received signal. This is achieved by folding the echo frequency samples at the index corresponding to the low receive bandwidth and by adding the terms that are superposed. In time-domain, the samples resulting from the CES are simply downsampled according to the lower bandwidth rate. In the same manner as for the other side, the purpose of such processing is to include the lowpass filtering action of the received analog-to-digital converter (ADC) into the echo channel estimate. In regards of the multi-rate aspect, Ysebaert *et al.* [6] reused the same general principle as above in their proposed EC.

1.2 Thesis contribution

As mentioned previously the aim of this thesis is to improve the speed of convergence and reduce the computational complexity of a DMT based echo canceller scheme. Each of these objectives will be achieved through different ideas.

It is possible to increase the speed of convergence of the echo canceller by initializing the frequency-domain echo channel coefficients to a better value than zero. The idea is to consider the convolution of the echo channel with the transmit signal as if it was a circular convolution, and then to solve a corresponding linear system of equations. In [1], a very similar algorithm is used in conjunction with a training sequence of two frames. In our proposed algorithm, no training sequence is required and the algorithm is performed on one frame only. As a result, our proposed method is much simpler in the sense that it does not require any protocol but is, however, less accurate. The fundamental basis of the algorithm is to benefit from the prefix of the transmit signal that helps making the linear convolution appear to be circular. It is possible to derive a theoretical approximation of the residual echo power after applying the initialization technique by analyzing the equations defining the power of the echo signal resulting from the application of the two kinds of convolution. The proposed initialization technique is applicable for single rate DSL as well as for multi-rate DSL.

As for the objective of reducing the computational complexity, a new technique is pro-

posed for the multi-rate case on the modem that transmits over the lower bandwidth. The idea is to avoid the adaptation processing related to the high frequency components of the echo channel for which the echo interference is below the noise floor. This is accomplished by setting the corresponding frequency coefficients to zero. Moreover, the zeroing of the coefficients leads to further computational complexity reduction by simplifying the IFFT of the frequency-domain echo channel. Indeed, by merging the pruned IFFT algorithm of [8] with the adapted IFFT algorithm for OFDM communication system described in [9], we can get an even lower computational complexity IFFT.

The performances of the proposed initialization technique will be verified through computer simulations in an ADSL-like communication system for different timing alignments between near-end and far-end signals. The effectiveness of the reduced complexity echo canceller algorithm will also be validated through computer simulations for different DAC lowpass filters.

1.3 Organization of thesis

The thesis is organized as follows. Chapter 2 presents some technical background required for the understanding of the thesis: overview of discrete multi-tone (DMT) modulation, description of a general DSL transmitter, description of DSL interference, and overview of ADSL and VDSL technologies. Chapter 3 presents the literature review related to echo cancellation in DMT-based DSL. The origin of the least mean square (LMS) formula and the derivation of the mean square error (MSE) equation are first explained in details. Afterwards, the chapter also reviews in more details the papers cited previously. Chapter 4 describes the two thesis innovations, namely, the fast initialization technique and the reduced complexity EC technique. Finally, Chapter 5 is devoted to the experimental results: the characteristics of the simulator are first explained, afterward the simulator is validated, and finally the simulation results for the two proposed techniques are presented. The last chapter summarizes the improvements brought by the thesis contributions and discusses their significance.

Chapter 2

Background

This chapter describes the DSL environment. The first section reviews the discrete multi-tone modulation (DMT) principles. The second section presents a general DMT based DSL transmitter and receiver. The two following sections introduce the origin of the echo interference and the notion of crosstalk interference. Finally, the last two sections present an overview of the characteristics of ADSL and VDSL technologies.

2.1 DMT review

In discrete multitone (DMT) modulation, the information is transmitted through independent tones (more commonly known as frequency subbands). Each of these contains one quadrature amplitude modulation (QAM) symbol called subsymbol. The principle behind DMT is to create a sequence of QAM subsymbols representing the entire frequency band and to perform an inverse fast Fourrier transform (IFFT) on the sequence. The resulting time-domain sequence is afterward serialized, passed into a digital to analog filter (DAC) and transmitted. Figure 2.1 illustrates the general process of DMT. X_n and x_k represent respectively the nth frequency subsymbol and the kth time-domain sample.

As it can be observed on the figure, to create a sequence of N real time domain data, a maximum of $N/2$ tones can be used. The reason for this is that the output sequence resulting of an IFFT usually possesses real and imaginary components. In the time-domain, it is not possible to express any imaginary components. Therefore, in order to get the sequence real, the IFFT inputs created from the frequency subsymbols need to be organized in this particular format: $[\Re(X_0), X_1, \ldots, X_{N/2-1}, \Im(X_0), X^*_{N/2-1}, X^*_{N/2-2}, \ldots, X^*_1]$ where

Input data
(0,1 sequence)

QAM
modulation

X_0
X_1
·
·
·
$X_{N/2-2}$
$X_{N/2-1}$

IFFT

X_0
X_1
·
·
·
·
·
X_{N-2}
X_{N-1}

P/S

Transmit filter
+ DAC

Output
(to the receiver)
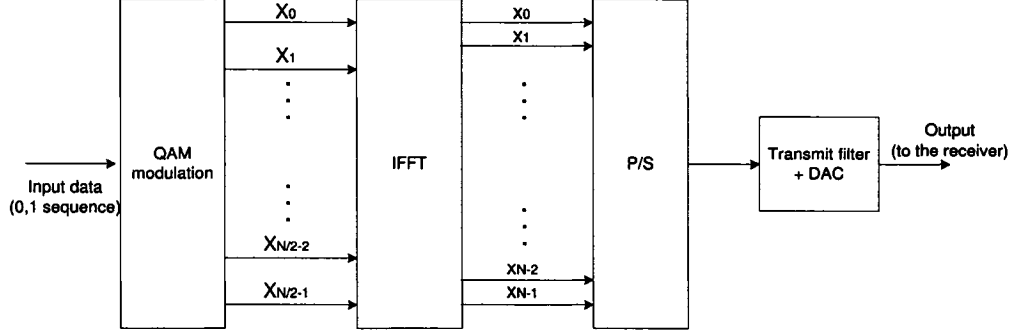
Fig. 2.1 Discrete multi-tone modulation.

* denotes complex conjugate and, $\Re$ and $\Im$ respectively denote the real and imaginary part of their argument. The tone X_0 is decomposed into its real and imaginary part which are assigned to the 1st and $(\frac{N}{2} + 1)^{th}$ IFFT inputs, so that the corresponding time-domain sequence is real [10].

Given that the tone frequency bandwidth is fixed and that the transmit power is limited, the remaining solution to increase the amount of information to transmit through the channel is to vary the QAM used on each tone according to the signal-to-noise ratio (SNR). Consequently, tones with high SNR are associated with high order QAM and vice-versa. A formula relating the SNR to the proper QAM can be found in [11].

Separating the frequency band into multiple tones diminishes the frequency variation of the channel over one transmit symbol. The aim of such doing is to have a very little variation of the channel over one tone so that the inter symbol interference (ISI) will also be small [11]. To illustrate the matter, suppose that we have a propagation channel as shown on Figure 2.2. Separating the channel bandwidth into tones corresponds to estimating the channel by rectangles as shown in Figure 2.3. A narrower subband (i.e. increasing N) translates into smaller ISI [1]. In fact, if the rectangles could follow exactly the channel (i.e. if N was infinite), the following equation would be true [11]:

$$U_n = G_n X_n \tag{2.1}$$

where U_n is the nth sample of the receive signal and G_n is the nth frequency response

---

[1]Reminder: a flat channel means no ISI.

element of the propagation channel.

Fig. 2.2   Example of propagation channel.
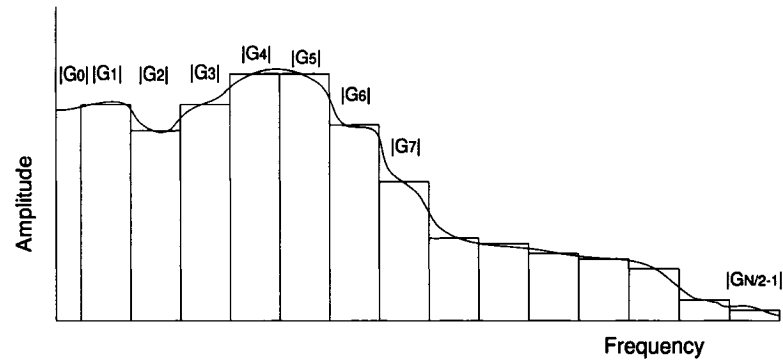
Fig. 2.3   Example of propagation channel divided into subbands.

The design of a DMT system depends on two inter-related factors, i.e. the latency and the channel. Indeed, a DMT system possesses latency because the demodulation of the receive signal is performed by blocks of N samples. This data is obtained at the sampling rate of the system which in turn is defined by the bandwidth of the channel frequency response. Moreover, the number of samples that defines the received signal block impacts the efficiency of the system since the overhead due to the prefix is fixed. In other words, the channel defines the maximum sampling rate to be used while the constraint on latency defines the maximum number of samples to include in the received signal block.

2.2 A general DMT based DSL transmitter/receiver

This section describes the particularities involved in a typical DMT-based DSL system. More precisely this section intends to explain the principle of the bit loading algorithms, the notions of prefix/suffix, the origin of the echo, and some brief characteristics of crosstalk interference. In regards to the receiver, the time-domain equalizer (TEQ) and frequency-domain equalizer (FEQ) are also going to be discussed briefly. As a basis for the upcoming explanations, the following figure illustrates a typical DMT-based DSL (e.g. ADSL) transmitter-receiver model. It should be mentioned that most DSL technologies use some sort of channel coding to counter interference, however this aspect is not relevant for the purpose of this work and thus we will limit the explanation about the receiver at the FEQ stage. In this thesis, we will refer to the modem located on the customer side as the remote terminal (RT) and to the modem located on the service provider side as the central office (CO).
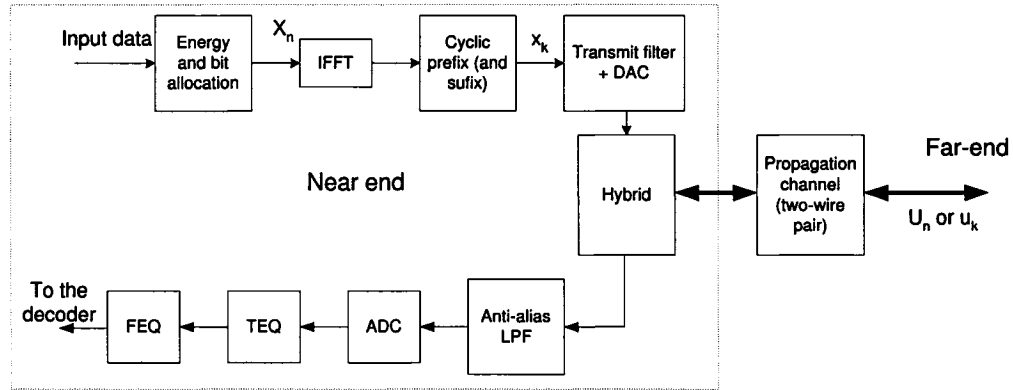
Fig. 2.4   DSL transmitter and receiver model.

2.2.1 Overview of bit loading

As shown on Figure 2.4, the determination of the number of bits to be carried on every tone is determined at the beginning of the transmission line. This process is referred to as the bit loading algorithm and depends on: the quality of the signal on the given frequency band [11], the power constraints, and sometimes the target bit rate. Briefly, high SNR tones can carry more bits than low SNR tones. So the bit loading table reflects the variation of the

SNR over frequency. Noise and channel conditions are constantly measured for each tone separately, to achieve optimal transmission at any time. The following equation expresses the number of bits that can be loaded into a tone [11]:

$$b_i = \log_2 \left(1 + \frac{\text{SNR}_i}{\Gamma} \right) \qquad (2.2)$$

where SNR_i is the signal-to-noise ratio for the ith tone, and Γ is the SNR gap. The latter is a measure of loss with respect to theoretically optimum performance. Equation (2.2) is an important part of the bit loading algorithm, however, it does not represent the whole algorithm since the overall power constraints of the transmit signal are not taken into account.

2.2.2 Origin of echo

In this model, it can be observed that the transmit ant receive paths are joined together at a four-wire to two-wire conversion hybrid for simultaneous transmission in both directions over the two-wire pair. The hybrid consists in an electrical bridge with one branch being the twisted-pair wire loop and the other branch being an electrical circuit. Ideally, the impedances of the two branches are identical and the separation of the signals is perfect. However, due to the variation of loop makeups, the hybrid is imperfectly matched. The consequence is that part of the near-end transmit signal appears at the receiver and acts as interference. This signal is commonly called echo. More details on echo transfer function can be found in [12].

2.2.3 Prefix and suffix

Back to Figure 2.4, we can notice an additional "prefix-suffix" box when compared with the transmitter part of Figure 2.1. To describe this additional processing, we first need to define the sample sequence resulting after the IFFT processing: $[x_0, x_1, \ldots, x_{N-1}]$. Adding a prefix of length L consists in taking the last L samples of the sequence and appending them to the beginning of the sequence such that now the sequence appears like this: $[x_{N-L}, x_{N-L+1}, \ldots x_{N-1}, x_0, x_1, \ldots, x_{N-1}]$. In contrast, adding a suffix of length S consists in taking the first S samples and appending them at the end of the sequence. The new sequence including the prefix and suffix is defined as $[x_{N-L}, x_{N-L+1}, \ldots x_{N-1}, x_0, x_1, \ldots, x_{N-1}, x_0, x_1,$

$\ldots, x_{S-1}]$.

The purpose of prefix and suffix addition is to suppress interference. In the case of the prefix, it facilitates the suppression of the channel frequency variation. Indeed, by preceding the useful receive block sequence by a sufficiently long prefix, the convolution between the propagation channel and the transmit signal appears as if it was a circular convolution, and thus the effect of the channel can be cancelled out by a simple (i.e. multiplicative) frequency equalizer (FEQ). In fact, the prefix allows equation (2.1) to be true as long as $L + 1$ is longer than the effective length of the propagation channel impulse response.

The purpose of the cyclic suffix addition is to avoid near-end crosstalk (NEXT) interference (see Section 2.2.5) and cross-echoing on both receiver sides (RT and CO). Indeed, without the use of the suffix, a typical block alignment between the receive and transmit signal might look like Figure 2.5. As it can be seen, a considerable discontinuity occurs in the signals between each transmitted frame. Consequently, when this portion of the transmitted signal is enclosed in the useful block FFT, the frequency representation of this signal gets modified and frequency leakage occurs. It follows that time-aligned orthogonal signals lose part of their orthogonality property when they are unaligned, which lead to NEXT and cross-echoing. The latter is defined as the portion of the echo interference signal that belongs to a frequency band different from that of the near-end signal.
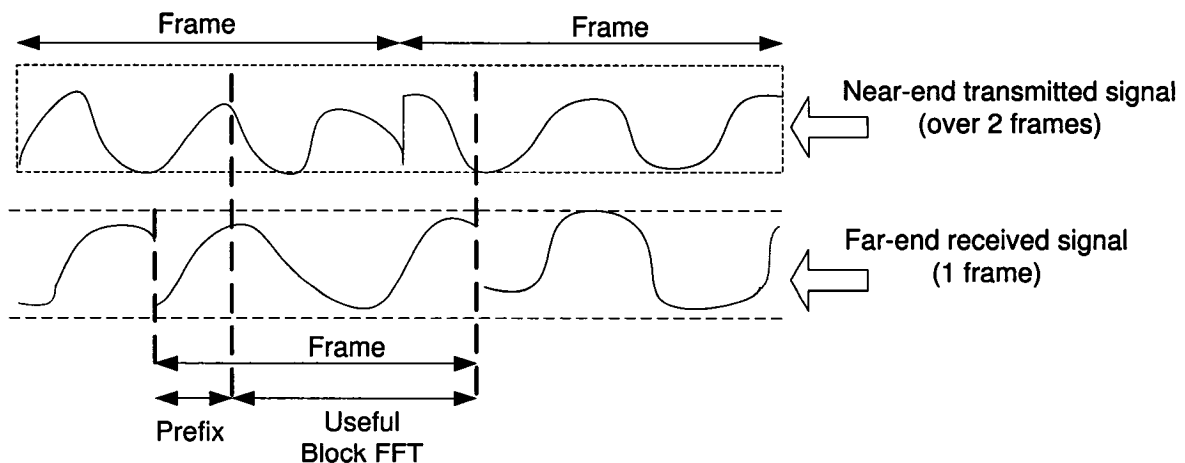
Fig. 2.5   Non-orthogonal NEXT.

The effectiveness of the suffix occurs when the transmit signals from the CO and RT are

sent at the same absolute time (this method is called timing advance). In the case where the suffix length of the receive signal is at least as long as the propagation delay due to the channel, the useful received block symbol (data portion) will always fall within the data of a unique transmit symbol coming from the near-end, as shown on Figure 2.6. In such a case, it is possible to use frequency division duplex (FDD) and omit the use of analog filter; this property was desired feature during the elaboration of VDSL technology.

Near-end transmitted signal

Far-end received signal

Prop. delay   Useful Block FFT
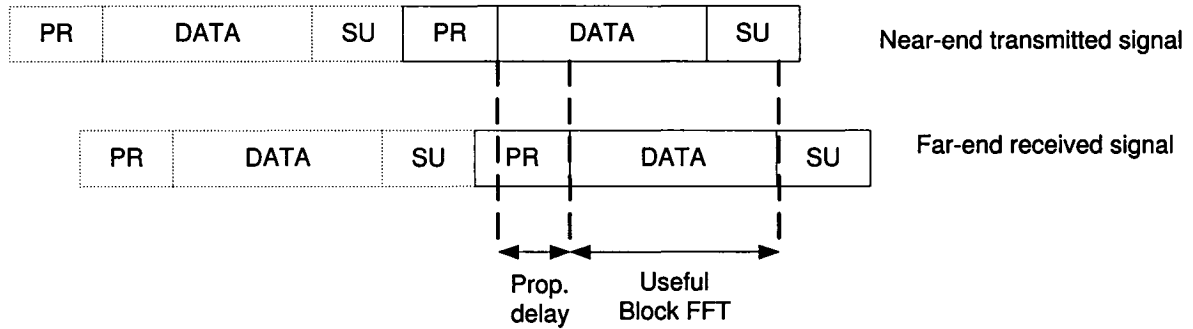
Fig. 2.6 Timing of the signals in synchronous VDSL.

2.2.4 Time-domain and frequency domain equalizer

The FEQ is composed of one tap for every tone. Its purpose is to scale and rotate the constellation on each subchannel so that a common decoder can be used on all subchannels. Given that the noise is embedded into the received signal coming from the far-end, during the FEQ processing, the noise gets scaled at the same. Thus, the FEQ does not yield to performance improvement and solely simplifies the decoder implementation [13].

On the other hand, the TEQ is used to improve the performance of the receiver. A wide variety of TEQ exists, e.g. generalized decision feedback equalizer and zero forcing algorithm [14–16], and considerable studies about TEQ for DMT systems are still ongoing. As mentioned in the previous subsection, the FEQ is not applicable if the effective length of the propagation channel impulse response is longer than the prefix length +1. In this particular case, the TEQ is also used to reduce the length of the propagation channel. Indeed, the channel perceived at the FEQ stage consists in the convolution of the propagation

channel with the TEQ coefficients; hence, it is possible to have a shorter perceived channel when compared with the original propagation channel.

2.2.5 Notion of crosstalk

A telephone cable can contain up to several thousands of twisted-pair copper wires. Since these wires are not shielded, each of them creates an electromagnetic field around itself. This field interferes with the electric signal travelling in the neighboring wires. This interference is called crosstalk. The fact of twisting the wire changes the orientation of the electromagnetic field and reduces the interference but does not remove it completely. Crosstalk can be classified into two types: near-end and far-end crosstalk.

Near-end crosstalk (NEXT) is defined as the interference coming from the same ends as that of the received signal. This means that for a signal received at the line terminal, near-end crosstalk is defined as the interference due to the signals coming from all other line terminals that use the same telephone cable for their transmission. A similar phenomenon is present at the central office side. Near-end crosstalk is a very important source of interference. One way to circumvent it is to use frequency division duplex (FDD). In this way, the interference coming from the near-end crosstalk will not belong to the frequency band of the received signal.

In contrast, far-end crosstalk (FEXT) is defined as the interference coming from the opposite side of the received signal end. Thus, for a signal received at the line terminal, far-end crosstalk is the electromagnetic interference due to the signals coming from the central office side, and vice-versa for a signal received at the central office side. In comparison with near-end crosstalk, far-end crosstalk is much less important because the FEXT interfering signal gets attenuated by travelling through the length of the twisted-copper wire line. However, when FDD is used to eliminate NEXT, FEXT becomes the major performance impairment in DSL. To ensure compatibility between the various DSL technologies, frequency spectrum masks are specified for each DSL standards.

As described in [17], the following equations, (2.3) and (2.4), show how to calculate the power spectrum of the crosstalk interferences. For the near-end crosstalk, we have

$$NEXT(f,n) = S(f) \; Q_{NEXT} \; n^{0.6} \; f^{3/2}(1 - |H(f,B)|^4), \qquad (2.3)$$

where $Q_{NEXT} = 8.536 \times 10^{-15}$, n = number of disturbers, f = frequency in Hz, B = NEXT

coupling length, $|H(f, l)|$ is the magnitude of the insertion gain transfer function for a loop length l, and $S(f)$ is the power spectrum of the interfering system at the initial point with the interfered system. As for the far-end crosstalk, we have

$$FEXT(f, n, l) = S(f) \ Q_{FEXT} \ n^{0.6} \ l \ f^2 \ |H(f)|^2, \qquad (2.4)$$

where $Q_{FEXT} = 7.74 \times 10^{-21}$, n = number of disturbers, f = frequency in Hz, l = FEXT coupling path length in feet, $|H(f)|$ is the magnitude of the insertion gain transfer function affecting the disturber signal, and $S(f)$ is the power spectrum of the interfering system at the initial point with the interfered system. The FEXT model assumes the insertion gain transfer function is computed for the total cable path located between the interfering transmitter and the victim receiver. On the other hand, the coupling loss is computed only over the coupling path length, i.e. l. The coupling path length is the length of cable over which the victim receiver and far-end disturbing transmitter have a common cable path.

2.3 ADSL

Created in 1999, ADSL stands for Asymmetric Digital Subscriber Line. It is a modem technology giving access to digital communication through the copper twisted pair telephone lines. The particularity of ADSL is the use of different transmission rates for downstream and upstream. Indeed, more than 8 Mbps downstream (to the customer) and up to 640 Kbps upstream can be transmitted depending upon the line length and the modem capabilities. Another property of ADSL is its capability to have voice communication over the plain old telephone service (POTS) at the same time as transmitting data on the telephone line. This characteristic combined with the fact that most of the home applications (such as internet download or full motion movie video) requires high data rate for downstream but relatively low data rates for upstream, makes ADSL a perfect contestant to fulfill the needs of residential customers. Another quality brought by ADSL consists of the increased distance that separate the central office from the customer terminal; the length of the twisted-pair copper line can reach as far as 5.5 km (as compared to 3.6 km for the previous HDSL2 technology [18]).

In North America, ADSL is defined under the ANSI T1.413 standard [19] and in Europe under the ITU G.992.1 [13]. To overcome the severe distortion of the copper line

and to counter the typical noise and impulses which exist in the residential twisted-wire pair environment, ADSL uses discrete multi-tone (DMT) for its transmission mode. The ADSL standards (ANSI and ITU) define 256 subchannels for the downstream data and 32 subchannels for the upstream. All subchannels have a bandwidth of 4.3125 kHz and no frequency guard band is needed between two successive channels. The available spectrum for downstream ranges from 25.875 kHz to 1.104 MHz, while for upstream it ranges from 25.875 kHz to 138 kHz. The low 25.875 kHz bandwidth is reserved for voice service (POTS). It follows from this that respectively 28 and 252 tones can be used to transmit data in the upstream and downstream. While the standards do allow full duplex in upstream frequency bands (optional), most of the operators avoid transmitting downstream data in the upstream band due to the increase in complexity that echo canceller requires.

2.4 VDSL

VDSL stands for Very high bit rates Digital Subscriber Line. This technology represents the latest in regards of DSL and can transmit up to 52 Mbps in downstream and up to 16 Mbps in upstream. This impressive data rates are achieved at the cost of reduced loop length. Indeed, the maximum loop length for VSDL is 1.2km which is much smaller than 5.5km for ADSL. This loop length reduction is achieved by replacing the main telephone line, going from the central office to the main junction box of a particular neighborhood, with fiber-optic cable. Thus, solely the distance between the customer and the junction box is linked by the twisted-copper-wire-pair. Reducing the loop length improves the quality of the twisted-copper-wire-pair signal and allows the use of a much higher frequency bandwidth.

In 2004, the American National Standard Institute (ANSI) finally defined VDSL under the standard *T1.424-2004* [20]. Until that, two VDSL modulation schemes were proposed: single carrier modulation (SCM) and multi-carriers modulation (MCM). The *T1E1.4* committee finally chose MCM as the modulation scheme to be used in VDSL. As a result, many ADSL characteristics are also present in the VDSL standard. For instance, VDSL uses DMT modulation with sub-carriers spacing of 4.3125 kHz. Some features like power back-off are also present.

Even though ADSL and VDSL are similar, considerable differences exist. The VDSL frequency band plan is as follows. Two frequency bandwidths for downstream are available: from 138kHz to 3.75MHz and from 5.2MHz to 8.5MHz. Similarly, upstream is also

composed of two frequency bandwidths: from 3.75MHz to 5.2MHz and from 8.5MHz to 12MHz. The frequency band going from 25kHz to 138kHz is available for either downstream or upstream and has to be negotiated during initialization. Other uses of the band, for instance echo cancellation mode, are for further study.

Another important modification when comparing VDSL with ADSL is the different use of the cyclic extension. VDSL uses both a prefix and suffix in the composition of its transmit signal. The purpose of the cyclic suffix addition is to avoid NEXT interference and cross-echoing on both receiver sides (RT and CO), as previously explained in section 2.2.3. To allow an effective usage of the suffix, VDSL can be deployed in synchronous or asynchronous mode. In synchronous mode, the timing advance technique is applied on all modems. More precisely, all modems on both sides that are transmitting through the same binder are synchronized together. By doing so, the properties of the suffix described in the previous sub-section become effective. In asynchronous mode, the timing advance technique is still performed but only on CO/RT pair by pair basis. This is to avoid cross-echoing interference, that otherwise would become too important at high frequencies.

In VDSL asynchronous mode, the NEXT interference is getting reduced by employing pulse shaping on the prefix and suffix, and furthermore, by employing special windowing on the useful FFT block [21]. Figure 2.7 demonstrates how such techniques makes the NEXT interference orthogonal. On the first DMT frame illustrated, no pulse shaping is applied and we can see that the discontinuity that occurs between two frames is embedded in the useful block FFT portion. This time-domain discontinuity corresponds to frequency leakage (out-of band) in the frequency-domain which explain the important NEXT that would result if no pulse shaping was applied. In the second set of sequence of DMT frames, we can see that by applying pulse shaping, the time-domain discontinuity disappears, which avoids frequency leakage and thus reduces the NEXT. In the third display, we have an example of what looks like a NEXT signal where pulse shaping was used. In the fourth display, the effect of windowing the receive signals can be seen on the NEXT signal; the extremity values of the NEXT signal in the useful block are zero, which is one of the characteristics of most types of window that can be applied (e.g. Tuckey, Bartlett and Lanczos). Windowing help to obtain high spectral containment.
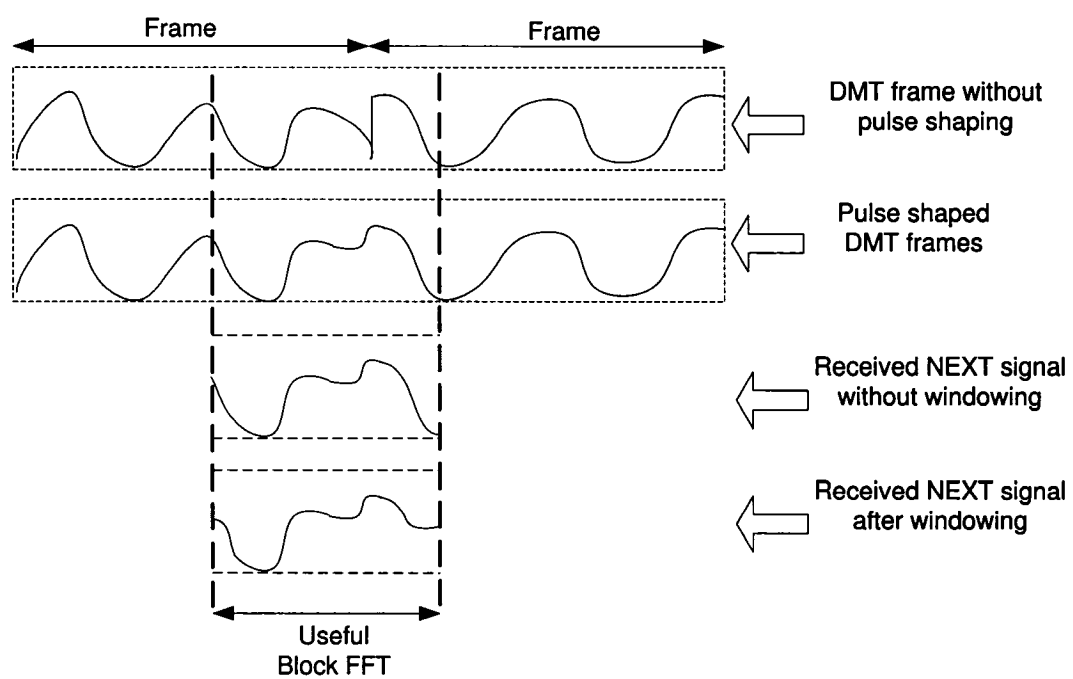
Fig. 2.7 Effect of pulse shaping and windowing on NEXT.

Chapter 3

Echo cancellation in DSL

The aim of this chapter is to present what has been accomplished up to now in the literature regarding echo cancellation and DMT technology. The first section gives some prerequisite information needed for the explanations of the diverse echo canceller structures that are presented in the following section. The third section is devoted to the particular case of multi-rate echo cancellation.

3.1 Prerequisites

This section first describes the origin and interactions of the various signals involved in the echo cancellation problem. The second subsection derives the formulation of the mean-squared error for a DSL system in which the echo channel can be estimated. The last subsection uses that error to derive the least mean square algorithm which is an integral part of most practical echo canceller systems.

3.1.1 Echo signal modelling

As depicted on Figure 2.4, the signal leaving the transmitter and creating the echo is represented by $x(t)$; it is constructed by modulating a series of data samples x_l by a transmit filter, or pulse shape $\Phi(t)$, i.e:

$$x(t) = \sum_{l=-\infty}^{\infty} x_l \Phi(t - lT), \tag{3.1}$$

where T is the sample period of the transmitter. As mentioned in Chapter 2, x_l is formed
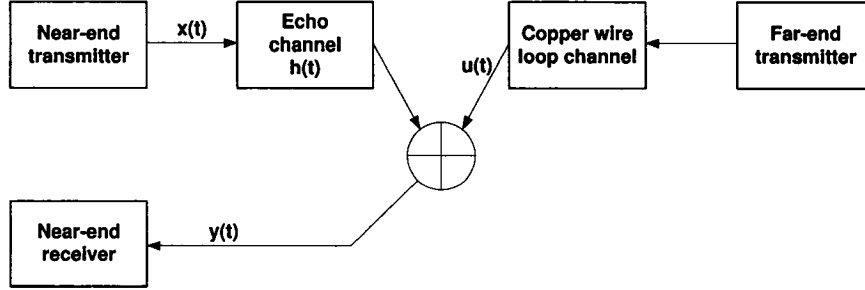
Fig. 3.1 Relation between far-end and near-end signals.

by the N-point IFFT of the frequency domain data symbols $\{X_i\}$. To comply with ADSL technology, the sequence x_l incorporates a prefix of L data samples for each transmitted symbol. In the following development, we will consider the case where the sequence x_l does not include any suffix. As illustrated in Figure 3.1, the signal received at the receiver $y(t)$ is composed of the far-end signal $u(t)$ added with an echo version of the transmitted signal $x(t)$. This can be expressed as

$$y(t) = \sum_{l=-\infty}^{\infty} x_l h(t - lT) + u(t), \tag{3.2}$$

where $h(t)$ is the combined impulse response of the transmit filter $\Phi(t)$ with the impulse response of the hybrid $h_y(t)$, or, $h(t) = \Phi(t) * h_y(t)$, where $*$ denotes continuous-time convolution. Assuming that the received signal is sampled at the rate of $1/T$, $h(t)$ can be represented as a causal filter h_m of M data sample length. Then, we can simplify (3.2) as

$$y_l = \sum_{m=0}^{M} h_m x_{l-m} + u_l \tag{3.3a}$$

$$= h_l * x_l + u_l \tag{3.3b}$$

in which $y_l = y(lT)$ and $*$ now denotes discrete-time convolution.

We can now relate the time index l with the symbol index i and the sample index k

within a symbol as follow:

$$l = (N + L)i + k \qquad k \in \{-L, N - 1\}, \ i \in \mathbb{Z}. \tag{3.4}$$

We introduce the vector $x_i = [x_{i,-L}, \cdots, x_{i,0}, \cdots, x_{i,N-1}]$ of length $N + L$ and refer to any particular data sample by $x_{i,k}$, where the corresponding time index is obtained from (3.4). It will be convenient to assume $k \in \mathbb{Z}$ and to set $x_{i,k} = 0$ for $k < -L$ and $k \geq N$. Similarly, the data samples corresponding to the far-end signal can be referred to as $u_{i,k}$. At the receiver, the total receive signal corresponding to the ith far-end transmit symbol is denoted by $y_i = [y_{i,0}, \cdots, y_{i,N-1}]^1$ in which a signal element can be referred to by $y_{i,k}$.

The echo interference in (3.3b) can be expressed [1] as

$$a_{i,k} \triangleq h * x \tag{3.5}$$

$$= \sum_{l=0}^{M-1} h_l x_{i,k-l} + \sum_{l=L+1}^{M-1} h_l x_{i-1,k+L+N-l} \tag{3.6}$$

$$= h_k * x_{i,k} + \overline{h}_k * x_{i-1,k+L+N}, \qquad k \in \{0, \cdots, N-1\}, \tag{3.7}$$

where

$$\overline{h}_k = \begin{cases} h_k & k = L + 1, \cdots, M \\ 0 & \text{elsewhere.} \end{cases} \tag{3.8}$$

The second term in (3.7) represents the echo component resulting from the previously transmitted symbol. Hence, the total received signal can be expressed as

$$y_{i,k} = a_{i,k} + u_{i,k} \tag{3.9}$$

$$= h_k * x_{i,k} + \overline{h}_k * x_{i-1,k+L+N} + u_{i,k}, \qquad k \in \{0, \cdots, N-1\}. \tag{3.10}$$

3.1.2 Mean-Square Error Analysis

Regardless of the particular echo canceller technique being used, the processing to remove the echo is essentially the same. We need first to estimate the echo channel response h_k through an adaptive algorithm based on the Mean Square Error (MSE). Then, secondly, we recreate the echo signal interference and subtract it from the received signal coming

---

[1]This signal is defined on solely N samples since it corresponds to the length of the receiver FFT.

from the far-end.

The MSE is quadratic in the echo channel estimate coefficients w_l and therefore has a unique minimum, which we call the MMSE estimate. To find it, we need to define the equation of the estimated echo based on (3.7) and (3.8) by, respectively, replacing h_k and $\overline{h}_k$ by w_k and $\overline{w}_k$:

$$\hat{a}_{i,k} = w_k * x_{i,k} + \overline{w}_k * x_{i-1,k+L+N}. \tag{3.11}$$

In the upcoming development, we will assume that the transmit signal $x_{i,k}$ and receive signal $u_{i,k}$ have zero-mean and are uncorrelated. We can now write the equation for the error by subtracting (3.11) from (3.10):

$$e_{i,k} = y_{i,k} - \hat{a}_{i,k} \tag{3.12}$$

$$= (h_k * x_{i,k} + \overline{h}_k * x_{i-1,k+L+N} + u_{i,k}) - (w_k * x_{i,k} + \overline{w}_k * x_{i-1,k+L+N}) \tag{3.13}$$

$$= (h_k - w_k) * x_{i,k} + (\overline{h}_k - \overline{w}_k) * x_{i-1,k+L+N} + u_{i,k} \tag{3.14}$$

Taking the mean square leads to

$$MSE = E\{|(h_k - w_k) * x_{i,k} + (\overline{h}_k - \overline{w}_k) * x_{i-1,k+L+N} + u_{i,k}|^2\} \tag{3.15}$$

$$= E\{|(h_k - w_k) * x_{i,k}|^2\} + E\{|(\overline{h}_k - \overline{w}_k) * x_{i-1,k+L+N}|^2\} + E\{|u_{i,k}|^2\}. \tag{3.16}$$

In the last equations, $|\ |$ represents the magnitude of the element located inside the bars, e.g. $|a + jb| = \sqrt{a^2 + b^2}$. The minimum of (3.16) occurs when $w_l = h_l$ for all $l = \{0, \cdots, M\}$, which results in a MMSE equal to

$$MMSE = E\{|u_{i,k}|^2\}. \tag{3.17}$$

3.1.3 Least-mean square algorithm

Considering that the MSE expression is quadratic in w_l, we can use this fact to develop a suitable adaptive algorithm. The methods of interest in this thesis are based on the Least Mean Square (LMS) algorithm in the frequency-domain. Since the echo channel is time varying, the algorithm is time adaptive, hence suffixed by symbol index i. The equation

for the update of the frequency-domain echo channel estimates takes the form [22]

$$W_{i+1} = W_i - \mu \nabla P(W_i), \tag{3.18}$$

where $W_i \in \mathbb{C}^N$ is a vector corresponding to the frequency-domain echo channel components, $\nabla P(W_i)$ is the gradient of the frequency-domain MSE cost function and μ is the step size. In order to derive an expression for $\nabla P(W_i)$, we need first to rewrite the MSE in the frequency-domain.

Let $E_{i,n}$ denote the nth element of the vector representing the FFT of the time-domain signal after being processed by the echo canceller, i.e. after that the estimated echo signal has been subtracted. In other words, $E_{i,n}$ is the remaining receive signal after echo cancellation. In [1], it is shown that $E_{i,n}$ can be expressed as

$$E_{i,n} = Z_{i,n} - W_{i,n}X_{i,n}, \tag{3.19}$$

where $Z_{i,n}$ represents the receive signal on which corrections have been made such that now the echo signal that is included in $Z_{i,n}$ appears as if it comes from a circular convolution between h_l and $x_{i,k}$, that is: $Z_{i,n} = U_{i,n} + X_{i,n}H_{i,n}$. This signal can be obtained by doing a N-point FFT for $k \in \{0, \ldots, N-1\}$ of the time-domain elements defined by:

$$z_{i,k} = y_{i,k} + \overline{h}_k * \tilde{x}_{i,k+N} - \overline{h}_k * x_{i-1,k+L+N}, \tag{3.20}$$

where $\tilde{x}_{i,k}$ is a windowed version of $x_{i,k}$ such that:

$$\tilde{x}_{i,k} = \begin{cases} x_{i,k} & k = -L, \cdots, N-L-1 \\ 0 & \text{elsewhere.} \end{cases} \tag{3.21}$$

It is now possible to write the expression of the mean square error:

$$MSE = P(W_{i,n}) = |E_{i,n}|^2 \tag{3.22}$$

$$= |Z_{i,n} - X_{i,n}W_{i,n}|^2 \tag{3.23}$$

$$= Z_{i,n}^*Z_{i,n} - Z_{i,n}^*X_{i,n}W_{i,n} - W_{i,n}^*X_{i,n}^*Z_{i,n} + W_{i,n}^*X_{i,n}^*X_{i,n}W_{i,n}. \tag{3.24}$$

By analogy, given that a quadratic equation of the form $P(C) = P_Y - D^*C - C^*D + C^*RC$

has a gradient $\nabla P(C) = 2RC - 2D$, we find that

$$\nabla P(W_{i,n}) = 2X_{i,n}^* X_{i,n} W_{i,n} - 2X_{i,n}^* Z_{i,n} \tag{3.25}$$

$$= -2X_{i,n}^* (Z_{i,n} - X_{i,n} W_{i,n}). \tag{3.26}$$

It can be observed that $Z_{i,n} - X_{i,n} W_{i,n}$ is in fact the frequency-domain error $E_{i,n}$ of equation (3.19), thereby, the expression of $\nabla P(W_{i,n})$ becomes

$$\nabla P(W_{i,n}) = -2X_{i,n}^* E_{i,n}, \tag{3.27}$$

where $X_{i,n}$ is the nth element of the vector representing the FFT of the near-end signal.

One should note that since the echo channel h_k is unknown, it is not possible to evaluate the signal $Z_{i,n}$, and thus, $E_{i,n}$ cannot be retrieved. However, it is possible to approximate very closely $Z_{i,n}$ by using the echo channel estimate $w_{i,k}$,

$$\hat{z}_{i,k} = y_{i,k} + \overline{w}_k * \tilde{x}_{i,k+N} - \overline{w}_k * x_{i-1,k+L+N}, \tag{3.28}$$

and thus, by replacing $Z_{i,n}$ with $\hat{Z}_{i,n}$ in the previous development.

Inserting (3.27) into (3.18) and using the approximate signal $E_{i,n}$, we obtain the following echo channel estimate update

$$W_{i+1,n} = W_{i,n} + \mu X_{i,n}^* E_{i,n}. \tag{3.29}$$

In the last equation μ absorbs the factor of -2 present in (3.27). The algorithm will converge for an initial condition of $W_{0,n} = 0$, $n = \in \{0, \cdots, N - 1\}$, provided μ is taken within the range $0 < \mu < 2$ [6]. Most of the differences between the various echo cancellers to be presented below reside in the way the different methods manage to obtain the error $E_{i,n}$. Therefore, the benefit of using this algorithm is the very low complexity while the drawbacks are a relatively slow convergence and the difficulties in getting the proper $E_{i,n}$.

3.2 Survey of recent developments in DSL echo cancellation

This section is devoted to the presentation of three echo canceller structures relevant for our work. In the optic of better understanding the echo canceller evolution, the EC are

presented in time order as they appeared in the literature. Therefore, the first one to be presented is from Cioffi *et al.* [1], it is followed by that of Ho *et al.* [2], and finally, the EC of Ysebaert *et al.* [6]. The required conditions to get an optimal echo canceller are summarized in a last subsection.

3.2.1 First echo canceller from Cioffi *et al.* [1] , 1994

One can say that the main thread regarding DMT based DSL echo cancellation started with [1]. The major breakthrough consisted of lowering the complexity inherent to signal driven echo canceller to a proper level by exploiting the structure of the DMT modulation. Indeed, the innovation, in regards of reducing the complexity, came with the idea of using the frequency-domain to update the echo estimator taps $w_{i,k}$. The basis of the algorithm was demonstrated in the previous subsection through equation (3.29).

In [1], to ensure that the frequency error used in (3.29) correspond to the true error coming from linear convolution, the authors used the time-domain echo channel estimates and convolved them with the time-domain near-end signals $x_{i,k}$ and $x_{i-1,k}$ just as it is done in (3.5). The recreated echo is then subtracted from the received signal as in (3.12). Figure 3.2 illustrates the echo canceller structure. More precisely, after each block update of the LMS algorithm, the echo canceller coefficients are inverse transformed to the time-domain for use in the time-domain convolution. Also, this set of coefficients are time-domain windowed by a rectangular window of length M to remove any double-talk noise that corresponds to time samples outside of the window of interest. Then $W_{i,n}$ is replaced by the transform of the windowed time-domain echo response. This has the effect of reducing the residual noise by a factor of $\alpha^2 = M/N$ [1].

3.2.2 An improved echo canceller version by Ho *et al.* [2], 1996

The previous structure [1] is efficient for low speed (sampling rates below 10 kHz) voiceband data modem. However, for higher sampling rates, the implementation of the finite impulse response (FIR) time-domain filter that synthesizes the echo becomes prohibitive. To solve the problem, a new DMT echo canceller is presented in [2]. The structure avoids most of the time-domain operations and cancels most of the echo in the frequency-domain directly.

To facilitate the manipulation of the echo canceller equations, we need to transform them into their matrix representations. We can redefine the echo signal described in (3.5)
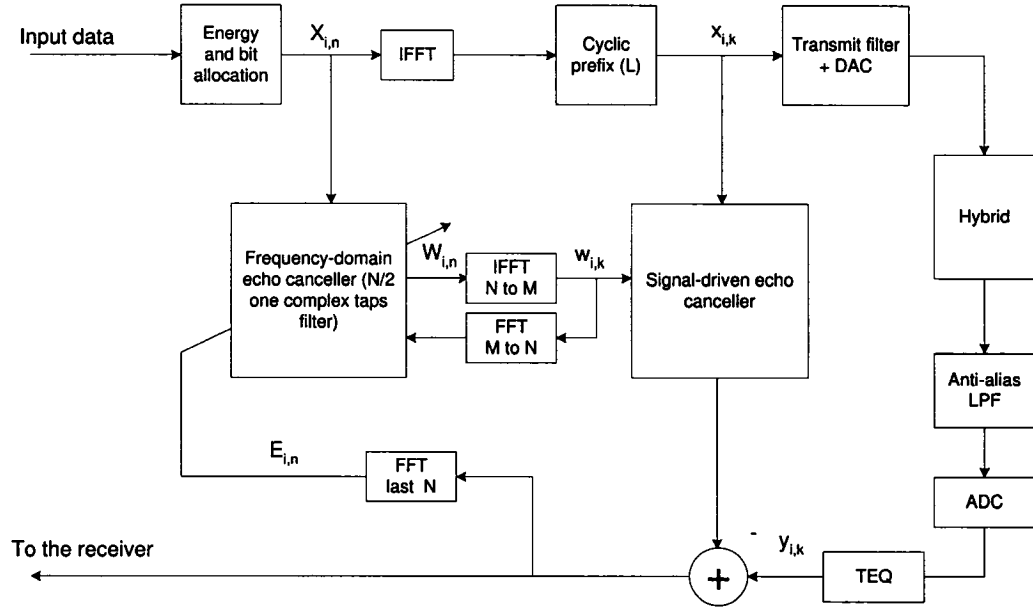
Fig. 3.2 Original echo canceller structure from [1].

as a vector of received data signal for symbol i,

$$a_i = T_{i,i-1}h \qquad (3.30)$$

with

$$T_{i,i-1} = \begin{bmatrix} x_{i,1} & x_{i,N} & \cdots & \cdots & x_{i,N-L+1} & x_{i-1,N} & \cdots & x_{i-1,L+2} \\ x_{i,2} & x_{i,1} & x_{i,N} & \cdots & & & & x_{i-1,L+3} \\ \vdots & & & & & & \ddots & \vdots \\ \vdots & & & & & & & x_{i-1,N} \\ \vdots & & & & \ddots & & & x_{i,N-L+1} \\ \vdots & & & & & & & \vdots \\ x_{i,N-1} & & & & & & & x_{i,N} \\ x_{i,N} & x_{i,N-1} & \cdots & & & & \cdots & x_{i,1} \end{bmatrix}. \qquad (3.31)$$

Here h is a vector representing the channel taps h_l and $T_{i,i-1}$ is a Toeplitz matrix composed

of the time-domain input data samples $x_{i,k}$ and $x_{i-1,k}$. In an effort to help the understanding of the matrix, the data vector that contains the $x_{i,k}$ is now defined as $[x_{i,1} \ldots x_{i,N}]$, with $x_{i,k} = 0$ for $k < 1$ or $k > N$.

Usually, $M > L+1$ and the model with the T matrix is needed. However, in the special case where $M \le L+1$, the linear convolution of (3.30) becomes a circular convolution, and the following circulant matrix C_i can replace matrix T in the sense that it generates the same N output samples

$$C_i = \begin{bmatrix} x_{i,1} & x_{i,N} & \cdots & x_{i,2} \\ \vdots & \ddots & \ddots & \vdots \\ x_{i,N-1} & & & x_{i,N} \\ x_{i,N} & x_{i,N-1} & \cdots & x_{i,1} \end{bmatrix}. \tag{3.32}$$

Circular convolution is equivalent to an element-by-element multiplication of the frequency-domain data symbol $X_{i,n}$ (obtained through FFT) with H_n. For the aim of our work we will consider the more general case $M > L+1$. However, C_i will still be used as a calculus artifact as we will demonstrate in the upcoming paragraphs.

Back to (3.30), taking the FFT of both sides gives

$$A_i = F_N T_{i,i-1} h, \tag{3.33}$$

where F_N is the matrix representing the N-point FFT. The idea here is to use C_i in combination with the frequency-domain processing to simplify the number of multiplies required in the echo canceller. This is done through

$$A_i = F_N(T_{i,i-1} - C_i + C_i)h \tag{3.34}$$

$$= F_N(T_{i,i-1} - C_i)h + F_N C_i h. \tag{3.35}$$

In the latter equation, the last term $F_N C_i h$ corresponds in fact to the FFT of the circular convolution defined by $C_i h$. Therefore, since time-domain circular convolution is equal to element-by-element multiplications in frequency-domain, we can state that $F_N C_i h = \text{diag}(X_i)H$, and we can rewrite (3.35) as

$$A_i = F_N \Omega_{i,i-1} h + \text{diag}(X_i)H. \tag{3.36}$$

The term $\Omega_{i,i-1}h$ with $\Omega_{i,i-1} \triangleq T_{i,i-1} - C_i$, represents the cross-echo,or equivalently, a short time-domain convolution operator that compensates for the difference between a linear and a circular convolution of the input data with the echo channel. Later on, this term will be referenced as the cyclic echo synthesizer (CES).

Replacing h by w_i, and, H by W_i, gives the two parts technique for the estimation of the echo signal, i.e.

$$\hat{A}_i = \text{diag}(X_i)W_i + F_N \Omega_{i,i-1} w_i. \tag{3.37}$$

Hence, we obtain the following matrix equation for the receive signal after subtracting the estimated echo,

$$E_i = Y_i - \hat{A}_i \tag{3.38}$$

$$= Y_i - \text{diag}(X_i)W_i - F_N \Omega_{i,i-1} w_i. \tag{3.39}$$

Figure 3.3 illustrates the echo canceller structure elaborated in [2] based on (3.39). The left middle box estimates the frequency domain echo taps just like it was already done in [1]. However, in regards of the echo signal emulation, the periodic echo signal is subtracted in the frequency domain instead of time-domain. The remaining echo left (cross-echo term or CES) is recreated in the right middle box and subtracted from the far-end received signal in the time-domain.

3.2.3 Optimizing alignment in echo cancellation, Ysebaert *et al.* [6], 2003

The echo canceller of [2] has very low complexity in terms of multiply operations. However, due to the propagation delay of the signals, it cannot be implemented on both the transmitter and receiver sides (remote terminal and central office). Indeed, it is only possible to synchronize the far-end signal with the near-end signal on one of the two sides. Without signal synchronization, the frequency data sample $X_{i,n}$, used for the estimation of the echo canceller frequency taps, belongs to two different symbols and therefore are not valid anymore.

In [6], to model the non-synchronized side, the authors redefine the matrix $T_{i,i-1}$ in order to include the integer delay Δ between the near-end transmit and receive signals. To comply with this new model, the matrix $T_{i,i-1}$ in equation (3.30) needs to be modified accordingly. Specifically, $T_{i,i-1}$ must be replaced by matrix $T_{i-1,i,i+1}$, now composed from
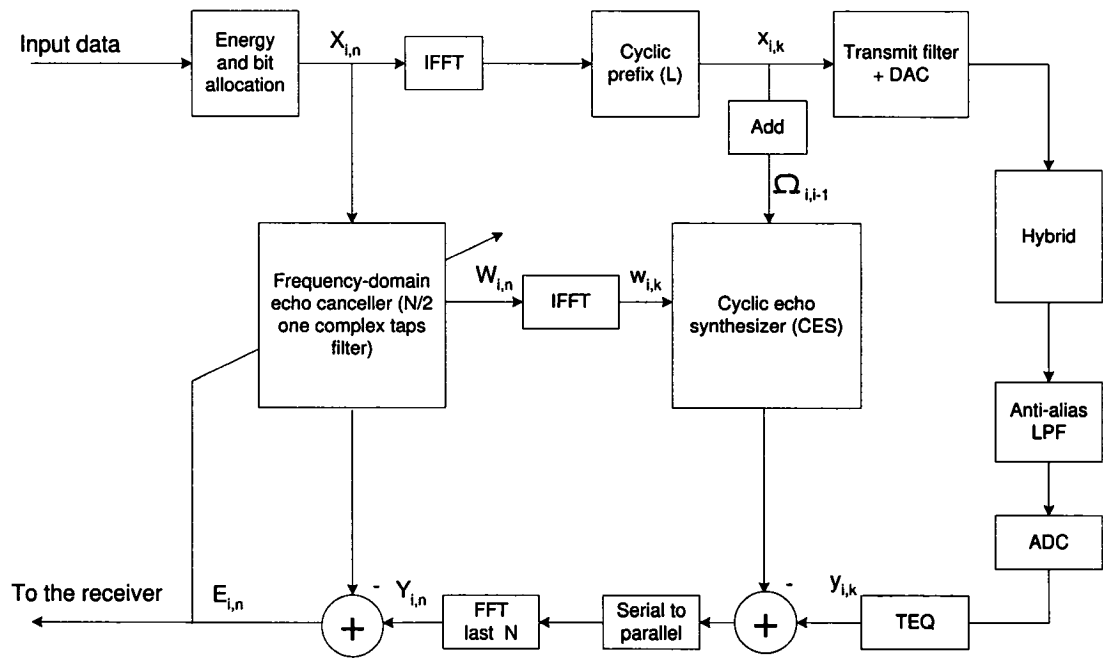
Fig. 3.3 Improved echo canceller from [2].

three consecutive symbols as follows [6]:

$$
T_{i-1,i,i+1} =
\begin{bmatrix}
x_{i,\Delta+1} & \cdots & x_{i,1} & x_{i,N} & \cdots & x_{i,N-L+1} & x_{i-1,N} & \cdots & x_{i-1,\Delta+L+2} \\
\vdots & \ddots & & \ddots & & & & & \vdots \\
x_{i,N} & \cdots & & & & & & \cdots & x_{i,1} \\
x_{i+1,N-L+1} & \cdots & & & & & & \cdots & x_{i,2} \\
\vdots & & & & \ddots & & & & \vdots \\
x_{i+1,N} & \cdots & & & & & & \cdots & x_{i,L+1} \\
x_{i+1,1} & \cdots & & & & & & \cdots & x_{i,L+2} \\
\vdots & & & & & & & \ddots & \vdots \\
x_{i+1,\Delta-L} & \cdots & & & & & & \cdots & x_{i,\Delta+1}
\end{bmatrix}
.
$$

(3.40)

In order to include matrix $T_{i-1,i,i+1}$ in equation (3.38), the calculus artifact C_i also needs to take into account the misalignment Δ. Therefore, C_i will be replaced by the circulant matrix $C_{i,\Delta}$ defined as follows:

$$
C_{i,\Delta} =
\begin{bmatrix}
x_{i,\Delta+1} & x_{i,\Delta} & \cdots & x_{i,2} & x_{i,1} & x_{i,N} & \cdots & x_{i,\Delta+2} \\
\vdots & \ddots & & & & & & \vdots \\
x_{i,N} & & & & & & & x_{i,1} \\
x_{i,1} & & & & & & & x_{i,2} \\
\vdots & & & & & & \ddots & \vdots \\
x_{i,\Delta} & x_{i,\Delta-1} & \cdots & x_{i,1} & x_{i,N} & x_{i,N-1} & \cdots & x_{i,\Delta+1}
\end{bmatrix}
.
$$

(3.41)

It can be observed that $C_{i,\Delta}$ is obtained by doing a circular shift of Δ elements on each of the columns of C_i.

We can then rewrite (3.38) as

$$
E_i = Y_i - F_N(T_{i-1,i,i+1} - C_{i,\Delta} + C_{i,\Delta})w_i \tag{3.42}
$$

$$
= Y_i - \mathrm{diag}(X_i)\mathrm{diag}(p)W_i - F_N\left((T_{i-1,i,i+1} - C_{i,\Delta})w_i\right). \tag{3.43}
$$

In the latter equation, the presence of $\mathrm{diag}(p)$ where the vector p is defined as $[1 \ \ldots \ e^{j2\pi\frac{i-1}{N}\Delta} \ \ldots \ e^{j2\pi\frac{N-1}{N}\Delta}]$ represents a phase shift. Indeed, we have established in (3.35) that $F_N C_i w = \mathrm{diag}(X_i)W_i$, and since in (3.43) C_i is replaced by $C_{i,\Delta}$ (a circular shift version of

C_i), then $F_N C_{i,\Delta} w = \text{diag}(X_i)\text{diag}(p)W_i$ due to the fact that a circular shift in time-domain corresponds to a phase shift in frequency-domain [10].

Alternatively, for the calculation of w_i, the multiplications related to the phase shift can be avoided by replacing them with a shift in the time-domain. Indeed, we can define $\tilde{W}_i = \text{diag}(p)W_i$ and apply an IFFT on it to obtain $\tilde{w}_i$. Hereafter, by doing a circular shift of Δ samples over $\tilde{w}_i$ allows w_i to be retrieved.

Back to (3.43), it is possible to reduce the complexity of both the RT and CO side by modifying $C_{i,\Delta}$. Indeed, we can define $\tilde{C}_{i,\Delta}$, a $N \times N$ circulant matrix in which its first column $\tilde{c}$ is composed of the first $N - N_b$ elements of the first column of $T_{i-1,i,i+1}$, concatenated with the N_b first elements (except the first one) of the first line of $T_{i-1,i,i+1}$ taken in reversed-order (see Figure 3.4), we thus have for the first column of $\tilde{C}_{i,\Delta}$:

$$\tilde{c} = [x_{i,\Delta+1} \cdots x_{i,N-N_b+\Delta}\ x_{i-1,N-N_b+L+\Delta+1} \cdots x_{i-1,N}\ x_{i,N-L+1} \cdots x_{i,N}\ x_{i,1} \cdots x_{i,\Delta}]. \quad (3.44)$$

Hence, $\tilde{C}_{i,\Delta}$ is constructed with N elements of the upper left corner of $T_{i-1,i,i+1}$. Now, using the same procedure as in the derivation of (3.42) and (3.34), the frequency-domain echo cancelled output can be expressed as

$$\begin{aligned}
E_i &= Y_i - F_N(T_{i-1,i,i+1} - \tilde{C}_{i,\Delta} + \tilde{C}_{i,\Delta})w_i \\
&= Y_i - F_N(T_{i-1,i,i+1} - \tilde{C}_{i,\Delta})w_i - F_N \tilde{C}_{i,\Delta}w_i \\
&= Y_i - F_N(\tilde{\Omega}_{i-1,i,i+1}w_i) - \text{diag}(\tilde{X}_i)W_i,
\end{aligned} \quad (3.45)$$

with $\tilde{\Omega}_{i-1,i,i+1} = T_{i-1,i,i+1} - \tilde{C}_{i,\Delta}$ and $\tilde{X}_i = F_N \tilde{c}$. The aim of introducing $\tilde{C}_{i,\Delta}$ is to obtain a matrix $\tilde{\Omega}_{i-1,i,i+1}$ composed of two triangles of non-zero elements. The minimum complexity in the CES (operations performed in the time-domain) occurs when the two triangles are symmetrical (same number of elements) [6]. This translates into the choice of $N_b = \frac{M}{2}$, where M is the useful length of the time-domain echo channel impulse response (IR). Indeed, as shown in Figure 3.5, the two useful triangles happen to be symmetrical and the last $N - M$ columns of the $\tilde{\Omega}_{i-1,i,i+1}$ are zeroed by the vector w_i during the matrix multiplications.

Depending on the choice of N_b, $\tilde{C}_{i,\Delta}$ can be composed of elements belonging to one or two symbols. In the case where $\tilde{C}_{i,\Delta}$ is composed of one symbol, we have $\text{diag}(\tilde{X}_i) = \text{diag}(X_i)\text{diag}(p)$. However, this relation is not true anymore in the case where $\tilde{C}_{i,\Delta}$ is

composed of two symbols, and thus an extra FFT on the vector $\tilde{c}$ is required.

It is possible to set $N_b = \frac{M}{2}$ and to align the transmit and receive signals such that $\tilde{C}_{i,\Delta}$ is composed of elements from solely one symbol, and thus the minimum complexity is achieved. However, since only one transceiver side can have its signals aligned, the other side will be misaligned and $\tilde{C}_{i,\Delta}$ will be composed of elements from two symbols. Given that the remote terminal (RT) transmits at a lower rate than the central office (CO), typically, the extra FFT implementation should be appointed to the RT since the additional FFT size is smaller. Figure 3.6 illustrates the echo canceller structures for the RT and CO sides as proposed by [6]; the dashed lines indicate the presence of the extra FFT required at the RT side. These echo canceller structures achieve much lower computational complexity than [1-5].
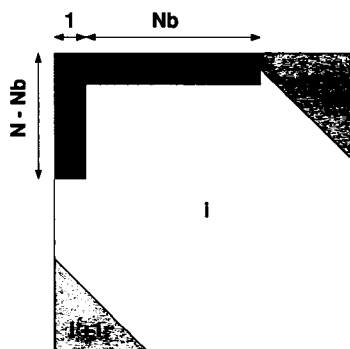
Fig. 3.4 How to get $\tilde{C}_{i,\Delta}$ from $T_{i-1,i,i+1}$.

Another improvement included in [6] consists in the implementation of double talk cancellation. Given that the FFT is shared between the demodulator and the echo canceller, we can now easily remove the far-end signal $U_{i,n}$ from the error signal $E_{i,n}$ by the use of a simple slicer error. In [4,5], it was proven that the advantage is a faster convergence of the EC coefficients. The double-talk canceller structure is illustrated at the bottom left in Figure 3.6.

3.2.4 Optimal echo canceller structure

In this subsection, we analyze the impact in terms of delays (alignment) for an optimum system. As mentioned previously, the alignment between far-end and near-end signals is
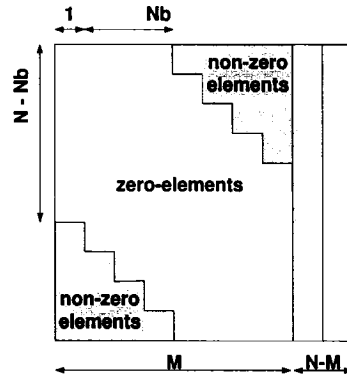
Fig. 3.5 Repartition of the zero and non-zero elements in $\tilde{\Omega}_{i-1,i,i+1}$.
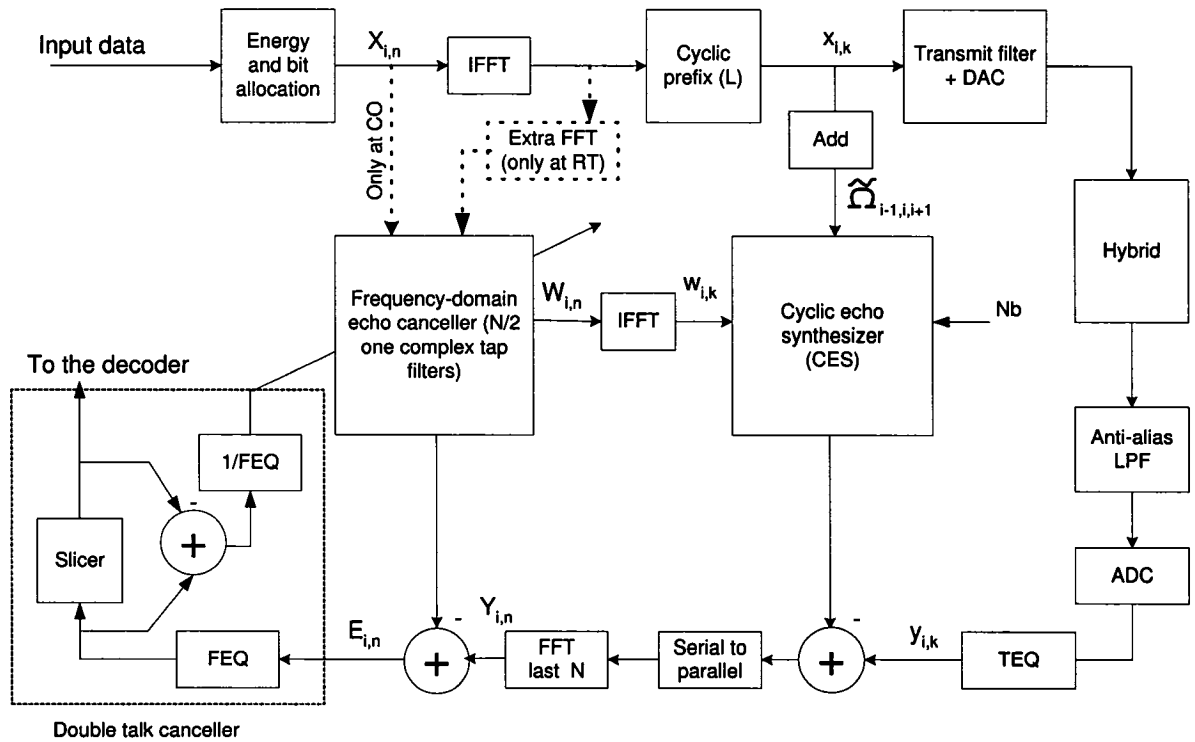
Fig. 3.6 Optimal echo canceller from [6].

going to be at CO side because of its bigger transmit FFT's size. As mentioned previously, the lowest computational complexity structure at the CO side is achieved when the optimal N_b is chosen and the transmit and receive signal are aligned such that $\tilde{C}_{i,\Delta}$ is composed of elements from one symbol instance. This is achieved by setting

$$N_b = \frac{M}{2}, \tag{3.46}$$

$$N_b \geq \Delta \geq N_b - L. \tag{3.47}$$

Regarding the definition of Δ, we will establish the transmit signal coming from the near-end as the reference. Therefore, a positive Δ means that the received signal from the far-end is late in comparison with the transmit signal from the near-end. This definition is in agreement with the Δ used in the definition of $T_{i-1,i,i+1}$.

To illustrate how the delays between far-end and near-end signals are related, Figure 3.7 shows an example of proper alignment. In this example, the number of tones is two, the prefix length is one (grey areas), the echo channel length is two, and the propagation channel delay is two. According to (3.46), N_b should be equal to one and therefore the delay at the CO be comprised in the interval $(1 \geq \Delta \geq 0)$; in the case illustrated on Figure 3.7, we chose one. The relation between the delay at the CO (Δ_{CO}) and the delay at the RT (Δ_{RT}) is given by

$$\Delta_{RT} = 2 * \Delta_{\text{channel}} - \Delta_{CO}, \tag{3.48}$$

with Δ_{channel} being the propagation delay of the channel. Hence, in our example, the delay at the RT is three. In [6], it is specified that an extra FFT would be required at the RT side to counter the misalignment of the signals.

3.3 Multirate echo canceller for ADSL

As mentioned in chapter 2, Asymmetric DSL (ADSL) transmits at a lower rate in the upstream than in the downstream direction. This particularity needs to be taken into account when designing the echo canceller. The first echo canceller structures adapted for the multirate case have been proposed in [2] and their general forms were reused in the improvement brought later on in [6].
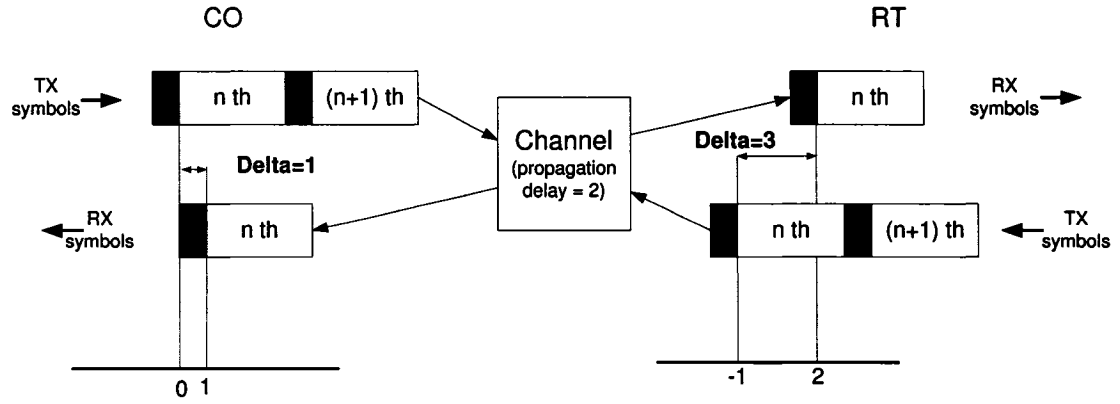
Fig. 3.7 Example of delays in an optimal alignment echo cancellation system.

3.3.1 Interpolated echo canceller on the RT side

In the case where the transmit signal has a smaller bandwidth than the receive signal, the approach described in [2,6], tries to annihilate the effect of the imperfect hybrid and imperfect DAC through the use of an echo canceller.

The use of the imperfect DAC at the transmission side results into the leakage of higher frequencies. Indeed, the signal coming from an imperfect DAC can be modelled as if the input signal was perfectly interpolated, and then lowpass filtered with cut-off frequency around the original transmit frequency.

For the purpose of simplifying the discussion, only the EC of [6] will be presented. The first step consists in interpolating the low frequency transmit signal to higher frequency. In the frequency-domain, this signal interpolation is simply performed by replicating $k - 1$ times the frequency data X_i, where k is the ratio between the transmit and receive signal bandwidth. To represent this operation in a mathematical form, X_i has to be multiplied by R, a block matrix consisting of k vertically stacked $N \times N$ identity matrices. In the frequency-domain, we now have the same number of data samples (kN) coming from the transmit signal and from the receive signal. As for the time-domain echo cancellation part, the data x_i also needs to be interpolated. This is done by padding $k - 1$ successive zeros between the successive data samples $x_{i,j}$. Figure 3.8 illustrates the ADSL echo canceller of [6] at the RT side. Once again, it can be noticed that the extra FFT has been assigned

to the RT side to reduce the computational complexity. In the same manner as in equation (3.45), the frequency-domain error sampled at the far-end transmit rate (higher rate) is given by:

$$E_i = Y_i - \text{diag}(R\tilde{X}_i)W_i - F_{kN}(\tilde{\Omega}_{i-1,i,i+1}w_i) \qquad (3.49)$$

where $\tilde{\Omega}_{i-1,i,i+1}$ is defined as in (3.40) but with $k-1$ zero padded between successive values, and $\tilde{X}_i = F_{kN}\tilde{c}$ with $\tilde{c}$ as defined in (3.44). The EC estimates the echo channel with solely $kN/2$ frequency taps since the second half of the frequency-domain signal is the complex conjugate data of the first half. As mentioned previously the echo channel estimates take into account the effect of the imperfect signal separation in the hybrid as well as the effect of the imperfect DAC operation. The taps are updated using the following equation:

$$W_{i+1} = W_i + \mu\text{diag}(R\tilde{X}_i^*)E_i. \qquad (3.50)$$
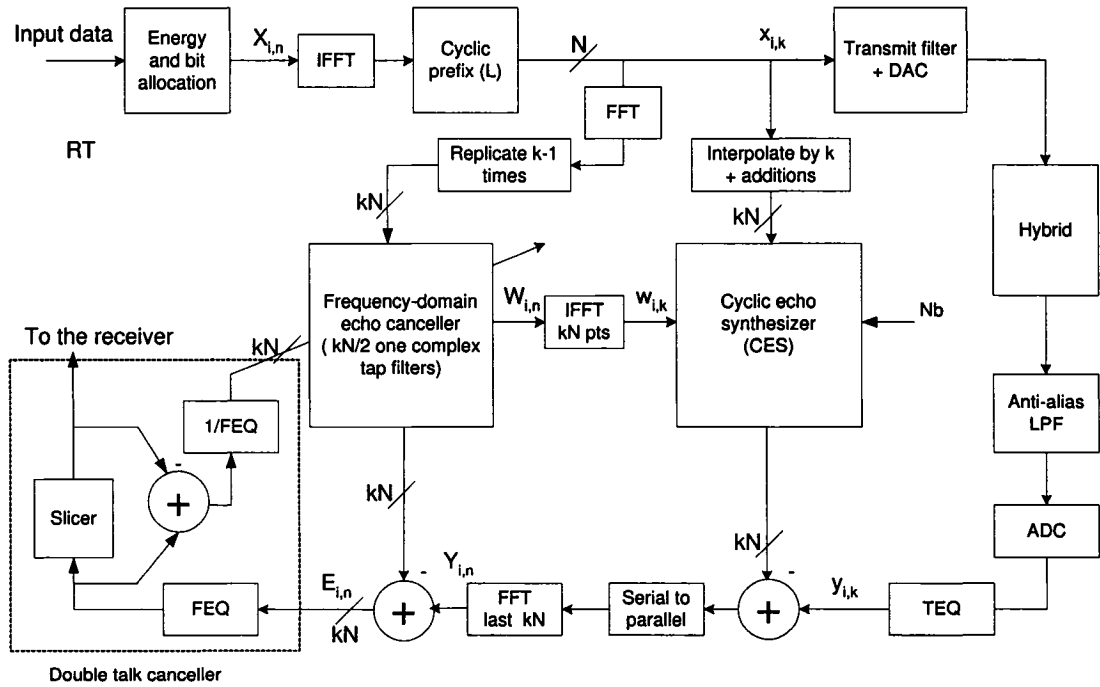
Fig. 3.8   Multirate ADSL echo canceller at RT with elimination of imperfect DAC.

3.3.2 Decimated echo canceller on the CO side

In contrast with RT, the transmit signal on the CO side has a k times larger bandwidth. Ideally, the anti-aliasing low-pass filter preceding the ADC of the receiver would block the higher frequency components. However, because it is not possible to build such a perfect filter, there is frequency aliasing that occurs when processing the received signal at the lower sampling rate. In the same manner as the interpolated echo canceller eliminates the imperfect DAC effect, the decimated echo canceller structure built in [2, 6] eliminates the aliasing interference by including its effects into the echo channel estimate.

In order to take into account the front-end lowpass filter, the frequency error vector E_i of the received signal is replicated $k - 1$ times to form a signal spreading over the whole bandwidth. The new created vector feeds the frequency-domain echo canceller part. As a result, the frequency-domain echo channel estimate is a vector of kN samples. Since the echo interference signal is aliased in frequency, the frequency-domain echo signal vector is then divided into k equal size vectors that are summed up together. This operation is labelled as the "Block and add" box of Figure 3.9 and is mathematically expressed by $R'\mathrm{diag}(X_i)W_i$, where R' is a matrix of k horizontally concatenated NxN identity matrices.

The time-domain part of the echo canceller only needs to compute one sample out of every k samples. This time-domain operation is indeed equivalent to frequency-domain aliasing. In other words, it corresponds to decimate the row of matrix $\tilde{\Omega}_{i-1,i,i+1}$ defined by (3.40), which means keeping every k^{th} lines of the matrix and removing the others.

The two operations are expressed mathematically by :

$$E_i = Y_i - R'\mathrm{diag}(p)\mathrm{diag}(X_i)W_i - F_{kN}(\tilde{\Omega}_{i-1,i,i+1}w_i). \tag{3.51}$$

In the same manner as in the single rate case, to minimize the overall complexity the optimal time alignment is performed on the CO side [6], therefore $\tilde{C}_{i,\Delta}$ comprises elements from a single symbol. The vector $p = [1 \ldots e^{j2\pi\frac{i-1}{kN}\Delta} \ldots e^{j2\pi\frac{kN-1}{kN}\Delta}]$ compensates for the possible phase shift between X_i and $\tilde{X}_i$. The frequency-domain adaptive weight coefficients are updated by:

$$W_{i+1} = W_i + \mu\mathrm{diag}(p)\mathrm{diag}(X_i^*)R'E_i. \tag{3.52}$$

The schematic structure of the decimated echo canceller is illustrated in Figure 3.9.
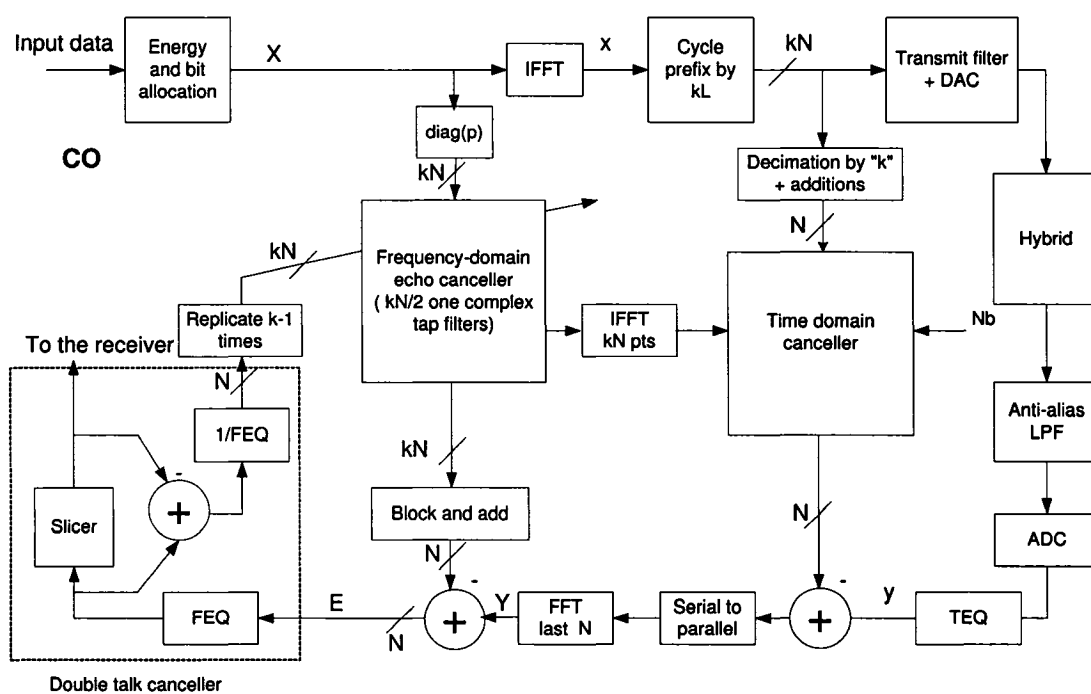
Fig. 3.9 Multirate ADSL echo canceller at CO.

Chapter 4

An improved echo canceller

This chapter presents the two contributions brought by this thesis. The first contribution improves the initial speed of convergence of the echo channel estimate used in the echo canceller. The second contribution aims to reduce the complexity of the multi-rate echo canceller at the remote terminal (RT) side. The chapter is divided into three parts; the first section presents the proposed initialization technique. The second section presents how to simplify the echo canceller by zeroing some frequency-domain echo channel components and by proposing a new IFFT scheme. Finally, the third section analyzes the computational complexity of our simplified echo canceller structure in comparison with that of [6].

4.1 A fast echo channel estimate

It is possible to accelerate the initial convergence of the echo canceller by replacing the first LMS iteration (equation (3.29)) by another adaptation equation in order to better initialize the echo canceller frequency-domain coefficients. Similarly to the fast start echo canceller of [1], the idea is to consider the convolution of the echo channel with the transmit signal as if it was circular. By doing so, it is possible to express and easily solve a corresponding MMSE equation. Given that the adaptation equation is applied only once at the beginning, we will omit the symbol index i in our discussion.

Under the assumption of circular convolution, the MSE can be written as

$$J(W) = ||U - \hat{U}||^2 = ||U - (Y - ZW)||^2, \tag{4.1}$$

where

$$Z = F_N C_{i,\Delta} F_N^{-1}. \tag{4.2}$$

In equation (4.1), $\| \; \|$ represents the norm of a vector. U and $\hat{U}$ are vectors containing respectively, the frequency samples of the far-end transmit symbol and those of the estimated far-end transmit symbol just before entering into the slicer of the receiver. Y is a vector of frequency-domain receive signal samples, i.e. the far-end transmit symbol corrupted with the echo interference signal. Z is in fact a diagonal matrix containing the frequency-domain samples of the transmit symbol on the near-end side multiplied by the proper phase to take into account the delay Δ. $C_{i,\Delta}$ is defined as in (3.41). One should note that to simplify the discussion, thermal noise and interference were not taken into account in (4.1); this does not affect the derivation. To find the MMSE solution, say W_o, we first rewrite $J(W)$ as follows

$$J(W) = a + W^H B + B^H W + W^H D W \tag{4.3}$$

where

$$a = \|U - Y\|^2 \tag{4.4}$$

$$B = Z^H(U - Y) \tag{4.5}$$

$$D = Z^H Z. \tag{4.6}$$

The vector W_o minimizing (4.3) is given by [22]:

$$W_o = D^{-1}B \tag{4.7}$$

$$= Z^{-1}(Y - U) \tag{4.8}$$

$$\simeq Z^{-1}E, \tag{4.9}$$

where it is assumed that none of the entries in Z are zero. In going from (4.8) to (4.9), we assume that the received far-end signal Y has sufficiently small echo interference so that the slicer decodes the proper far-end transmit signal, thereby allowing us to state $Y - U = E$, where E is the same as defined in the previous chapter. Since Z is a diagonal matrix, the computation of Z^{-1} is very simple; it corresponds to the element-by-element inverse. Therefore, applying the new equation in the model takes only four multiply oper-

ations per frequency coefficient as compared to six for one conventional least mean square (LMS) adaptation iteration (equation 3.29). This initialization technique is applicable for symmetric rate DSL as well as for multi-rate DSL.

The difference between this initialization scheme and the one explained in [1] is that, here, no initialization protocol is required. Indeed, in [1], the authors established a protocol to silence the double-talker coming from the far-end while at the same time the transmit signal sent is a pseudorandom (or chirp) training sequence of two frames. By doing so, [1] retrieves almost perfectly the echo channel. Therefore, the advantage of our proposed technique is that no protocol is required, which simplifies the initialization, while the drawback is a slower convergence since it does not retrieve the echo channel coefficients as well.

The performance of the proposed initialization technique depends on the approximation of the linear convolution by a circular one. We can identify three factors that have an influence on this approximation:

- the relative lengths of the prefix (L), of the echo channel impulse response (M), and of the FFT (N),

- the misalignment between the transmitted and received symbol,

- the shape of the echo channel impulse response.

Below, these factors are discussed individually.

The fact that DMT modulation in DSL includes a prefix tends to favor the above technique. For example, in the case where perfect alignment between the transmit and receive signal occurs, if the length of the echo channel impulse response is shorter than the prefix length, there will be no difference between linear and circular convolution. We can thus state that since the prefix length is fixed, the proposed algorithm will perform better for shorter echo channel impulse response. The length of the FFT is also a relevant factor since when the ratio of the FFT length over the echo channel IR length increases, the difference between circular and linear convolution decreases.

In regards to the alignment between the transmit and receive symbols, when the misalignment (delay $\Delta \geq 0$) is shorter than $M - L$, the prefix contributes to make the two kinds of convolution to appear the same. However, as it will be demonstrated below, the proposed scheme performs better as the delay is reduced.

Finally, as for the shape of the echo channel impulse response, in the case of perfect alignment, if most of the energy of the echo channel impulse response is concentrated on the L first taps, then, the circular convolution will very closely approximate the linear convolution. In other words, in the case that the echo channel impulse response has a long tail, the high length of this echo channel has a much reduced effect since most of the significant taps of the channel are used in the common multiplications that are required during the calculation of the circular and linear convolutions. Figure 4.1 illustrates the effects of the shape of the echo channel.
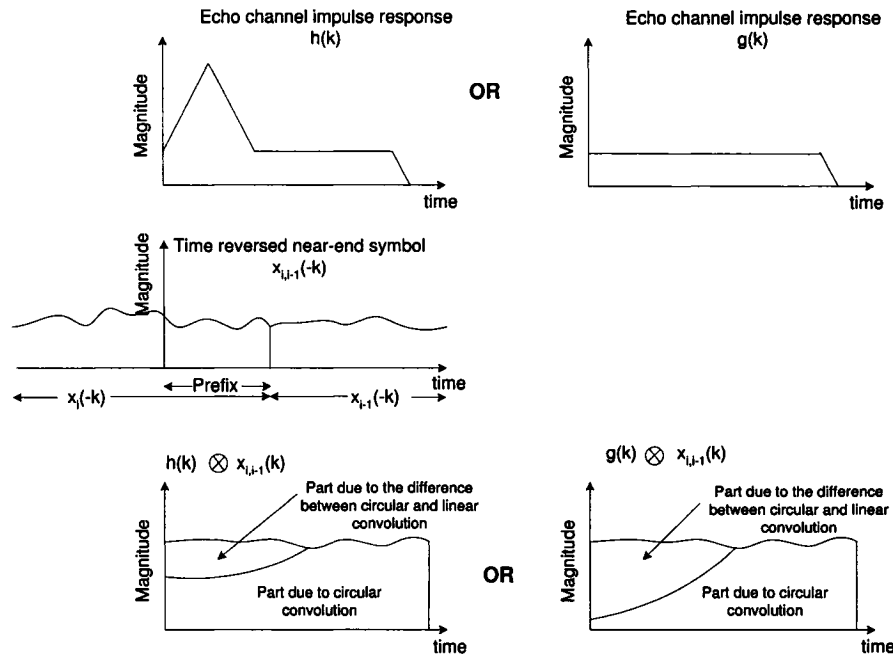
Fig. 4.1 Conceptual comparison of the magnitude composition of two different echo signals.

In the upcoming paragraphs, we derive a theoretical value to quantify the improvement in term of residual echo signal power left in the system after applying (4.9). First, we need to recall the definition of the time-domain echo signal for a block of N samples:

$$a_i = T_{i-1,i,i+1}h, \tag{4.10}$$

where $T_{i-1,i,i+1}$ is defined as in (3.40) and h is the time-domain echo channel vector zero

padded to length N. Given that we are neglecting the noise, we have $A_i = E$. Similarly, we can find the recreated echo signal after the application of (4.9):

$$b_i = T_{i-1,i,i+1} w_o, \tag{4.11}$$

where

$$w_o = F_N^{-1} W_o \tag{4.12}$$

$$= F_N^{-1} Z^{-1} E \tag{4.13}$$

$$= F_N^{-1} F_N C_{i,\Delta}^{-1} F_N^{-1} (Y - U) \tag{4.14}$$

$$= C_{i,\Delta}^{-1} F_N^{-1} F_N T_{i-1,i,i+1} h \tag{4.15}$$

$$= C_{i,\Delta}^{-1} T_{i-1,i,i+1} h. \tag{4.16}$$

We can now write the square norm of $a_i - b_i$ as:

$$||a_i - b_i||^2 = ||T_{i-1,i,i+1} h - T_{i-1,i,i+1} w_o||^2 \tag{4.17}$$

Putting (4.16) into (4.17), we get:

$$||a_i - b_i||^2 = ||T_{i-1,i,i+1} h - T_{i-1,i,i+1} C_{i,\Delta}^{-1} T_{i-1,i,i+1} h||^2 \tag{4.18}$$

$$= ||(I - T_{i-1,i,i+1} C_{i,\Delta}^{-1}) T_{i-1,i,i+1} h||^2 \tag{4.19}$$

We can replace the middle term $T_{i-1,i,i+1}$ by $C_{i,\Delta} + \Omega_{i-1,i,i+1}$ as previously defined in (3.45) and we get:

$$||a_i - b_i||^2 = ||(I - (C_{i,\Delta} + \Omega_{i-1,i,i+1}) C_{i,\Delta}^{-1}) T_{i-1,i,i+1} h||^2 \tag{4.20}$$

$$= ||(I - C_{i,\Delta} C_{i,\Delta}^{-1} - \Omega_{i-1,i,i+1} C_{i,\Delta}^{-1}) T_{i-1,i,i+1} h||^2 \tag{4.21}$$

$$= || - \Omega_{i-1,i,i+1} C_{i,\Delta}^{-1} T_{i-1,i,i+1} h||^2 \tag{4.22}$$

$$= || - \Omega_{i-1,i,i+1} w_o||^2 \tag{4.23}$$

The residual echo power left in the system after applying (4.9) can then be written as:

$$P_{res} = \frac{1}{N} E\{||a_i - b_i||^2\} \tag{4.24}$$

$$= \frac{1}{N} E\{|| - \Omega_{i-1,i,i+1} w_o||^2\} \tag{4.25}$$

We would also like to find a theoretical value that we could multiply with the power of the original echo signal such that it would give us the power of residual echo signal after applying our technique, i.e.

$$P_{ratio} = \frac{P_{res}}{P_{echo}}, \tag{4.26}$$

where P_{echo} is the power of the echo signal given by:

$$P_{echo} = \frac{1}{N} E\{||a_i||^2\}. \tag{4.27}$$

Using (4.10) and (4.25), we find that

$$P_{ratio} = \frac{E\{|| - \Omega_{i-1,i,i+1} w_o||^2\}}{E\{||T_{i-1,i,i+1} h||^2\}} \tag{4.28}$$

$$= \frac{E\{w_o^H \Omega_{i-1,i,i+1}^H \Omega_{i-1,i,i+1} w_o\}}{E\{h^H T_{i-1,i,i+1}^H T_{i-1,i,i+1} h\}} \tag{4.29}$$

It is possible to approximate the latter equation by posing some assumptions. First of all, we will assumed that the vector w_o is independent of $\Omega_{i-1,i,i+1}^H \Omega_{i-1,i,i+1}$, which allow the expected value of w_o to be taken apart. We can then approximate $E\{w_o\}$ by

$$E\{w_o\} = E\{C_{i,\Delta}^{-1} T_{i-1,i,i+1} h\} \tag{4.30}$$

$$= E\{C_{i,\Delta}^{-1} (C_{i,\Delta} + \Omega_{i-1,i,i+1}) h\} \tag{4.31}$$

$$= E\{h + C_{i,\Delta}^{-1} \Omega_{i-1,i,i+1} h\} \tag{4.32}$$

$$\tag{4.33}$$

and thus, by neglecting the term $E\{C_{i,\Delta}^{-1}\Omega_{i-1,i,i+1}h\}$ we get

$$E\{w_o\} \simeq E\{h\} \tag{4.34}$$

$$\simeq h. \tag{4.35}$$

Equation (4.29) now becomes

$$P_{ratio} \simeq \frac{h^H E\{\Omega_{i-1,i,i+1}^H \Omega_{i-1,i,i+1}\}h}{h^H E\{T_{i-1,i,i+1}^H T_{i-1,i,i+1}\}h} \tag{4.36}$$

To evaluate the expected values of the middle terms in (4.36), we will assume that the time-domain samples from which are composed $\Omega_{i-1,i,i+1}$ and $T_{i-1,i,i+1}$ are independent and identically distributed with zero mean and σ^2 variance. Thus, the computation of $T_{i-1,i,i+1}^H T_{i-1,i,i+1}$ gives a Toeplitz matrix for which the expected value gives a diagonal matrix where each element of the diagonal is equal to $N\sigma^2$.

Similarly, the computation of $\Omega_{i-1,i,i+1}^H \Omega_{i-1,i,i+1}$ gives also a Toeplitz matrix. However, since the non-zero elements of $\Omega_{i-1,i,i+1}$ are the summation of two samples belonging to different frames, the expected value of $\Omega_{i-1,i,i+1}^H \Omega_{i-1,i,i+1}$ gives a diagonal matrix where the elements of the diagonal are: $2\sigma^2 \times [\Delta \ (\Delta - 1) \ \dots \ 1 \ 0 \ \dots \ 0 \ 1 \ 2 \ \dots \ (N - L - \Delta - 1)]$. It is now possible to solve equation (4.36) and thus, to approximate P_{ratio}.

4.2 Low complexity EC at the RT side

In this section, the simplifications regarding the echo canceller algorithm are presented. The first simplification consists in setting to zero the echo channel estimated taps corresponding to high frequency in the case of multirate communication, specifically at the side that transmit at the lower rate. The second simplification relates to the use of an improved IFFT algorithm that has a lower computational complexity in the case where a small portion of the signal frequency components are non-zero.

4.2.1 Zeroing the high frequency echo channel taps

As mentioned in chapter 3, the echo channel estimated by the frequency echo canceller (FEC) consists in, as illustrated in figure 3.8, the convolution of three components: the

lowpass filter impulse response of the near-end DAC, the channel impulse response of the hybrid, and the TEQ. Due to the fact that convolution in time corresponds to multiplication in frequency; the magnitude frequency response of the echo channel is greatly impacted by the particular frequency response of the DAC lowpass filter. As a result, the magnitude response of the compounded echo channel decays significantly above the cutoff frequency of the DAC. Based on this interpretation, it appears justified to approximate to zero the high frequency components of the echo channel where the echo power is less than that of the noise floor. Figure 4.2 illustrates the general form of the magnitude frequency response of the compounded echo channel.

Instead of adapting the whole $kN/2$ frequency taps, the idea that we propose is to adapt solely the first s frequency taps and approximate to zero the remaining taps. The starting frequency index s where the zeroing begins has to be higher than the frequency bandwidth of the transmit near-end signal (which corresponds to the $\frac{N}{2}^{th}$ taps) and has to take into account the leakage implied by the DAC filter. Indeed, depending on the DAC filter performance; more or less leakage occurs. Big leakage requires the use of a higher value of s.

Applying this approach in a noise-free environment would reduce the system performance. However, this will not be the case in real environment, mainly because of the near-end crosstalk (NEXT) and far-end crosstalk (FEXT) interference. Indeed, as long as the residual echo level is below the actual interference plus noise level, this approach does not degrade the system performance. In fact, as it will be demonstrated in chapter 5, the proposed approach improves the system performance.

Indeed, looking back at figure 4.2 we can see that above the sth frequency component, the magnitude of the interference plus noise is higher than that of the echo signal. As a result, the EC of [6] can not differentiate the echo channel components from the interference, and thus, the operation of the adaptive EC acts as if it was trying to track the interference plus noise. It follows that the echo channel components estimated by the EC above the sth frequency component are erroneous. Consequently, the EC of [6] injects interference in the system instead of subtracting echo signal.
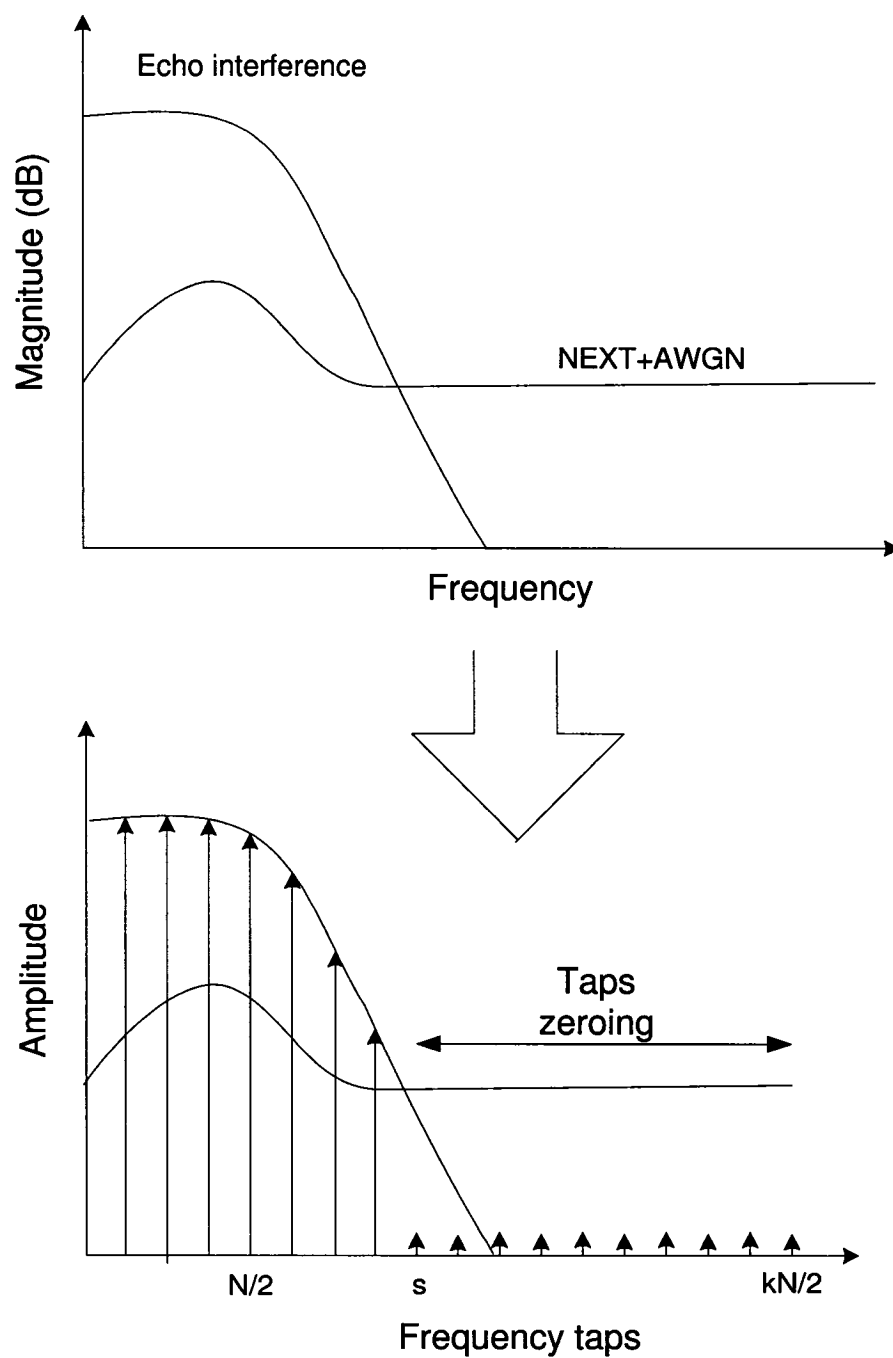
Fig. 4.2   Approximation to zero of the taps above index s.

4.2.2 Modified IFFT

One of the most time-consuming operations involved in DMT echo canceller regards the IFFT of echo channel estimate. In [9], Wu *et al.* addressed this issue by developing a low computational complexity IFFT algorithm especially designed for DMT communications. The benefit comes from the fact that the IFFT output is real which confer a special structure to the signal frequency samples. More precisely, a vector W of frequency samples corresponding to a real time-domain sequence containing kN samples possesses the following symmetry: $W_n = W_{kN-n}^*$ for $n = \{1, 2, \ldots, kN/2 - 1\}$. Furthermore, W_0 and $W_{kN/2}$ have to be real.

The algorithm proposed in [9] takes the first half of the input and applies on them a modified discrete cosine transform (MDCT) as well as a modified discrete sine transform (MDST). The particularity of these transforms is that they can be applied recursively in the same manner as the radix 2 is applied recursively on any FFT of power of 2 length, while at the same time their structure benefits from the symmetrical conjugate property of W.

It is also possible to exploit the fact that the high frequency components of the estimated echo channel are set to zero. In [8], Sorensen *et al.* developed a method, named transform decomposition, that simplifies the computational complexity of an IFFT in the case where a large portion of the last samples of the IFFT input vector are set to zero. The method consists in using solely the first s non-zero elements of the input, to scale them with some proper coefficients such that now instead of performing a kN-point IFFT, the transform decomposition method performs Q P-point IFFTs, where $P \geq s$ and $P \times Q = kN$.

The vector that represents the FFT of the echo channel estimate can be expressed as : $[W_0 \ W_1 \ldots W_{s-1} \ 0 \ldots 0 \ W_{s-1}^* \ldots W_1^*]$. The structure of this IFFT vector presents the special DMT structure required in [9], and also presents many zeros in the middle of the input vector which is almost as in [8] (the zero elements are solely at the end of the vector). Therefore, the IFFT scheme that we propose consist of applying the transform decomposition method of [8] over the MDCT-MDST schemes described in [9]. The next paragraphs explain how to proceed.

The following equations [1] define the MDCT and MDST used in a kN-point IFFT of

---

[1]To make the equation clearer, we will omit to specify the symbol index i in the following developments.

W.

$$MDCT(m) = \sum_{n=0}^{s-1} W_n^R \cos\left(\frac{2\pi nm}{kN}\right),$$ (4.37)

$$MDST(m) = \sum_{n=0}^{s-1} W_n^I \sin\left(\frac{2\pi nm}{kN}\right),$$ (4.38)

where W_n^R and W_n^I represent respectively the real and imaginary part of W, and $m = [0, 1, \ldots, kN - 1]$. As it can be observed, only the first s elements of W are required. Indeed, the other elements of W are either zero (which does not require any calculation), or conjugate-symmetric (which is taken into account in the MDCT-MDST definition).

Due to the conjugate-symmetric property of the vector, the kN-point IFFT of W can thus be written as

$$w_m = 2[MDCT(m) + MDST(m)],$$ (4.39)

Furthermore, by using the symmetrical and anti-symmetrical properties of the cosine and sine functions, we find that

$$MDCT(m) = MCDT(kN - m)$$ (4.40)

$$MDST(m) = -MDST(kN - m)$$ (4.41)

and thus only half of the MDCT (and MDST) output points need to be computed. To benefit from the fact that the summation in (4.39) goes only up to $s-1$ and not to $kN/2-1$, the transform decomposition method of [8] is now applied to the IFFT. Figure 4.3 illustrates the global scheme of our proposed IFFT.

Defining $C_{kN}^i = \cos(\frac{2\pi i}{kN})$ and similarly $S_{kN}^i = \sin(\frac{2\pi i}{kN})$, we first express the MDCT as

$$MDCT(m) = \sum_{n=0}^{s-1} W_n^R C_{kN}^{nm}.$$ (4.42)

Now using the transform decomposition method, we can introduce the variables P and Q
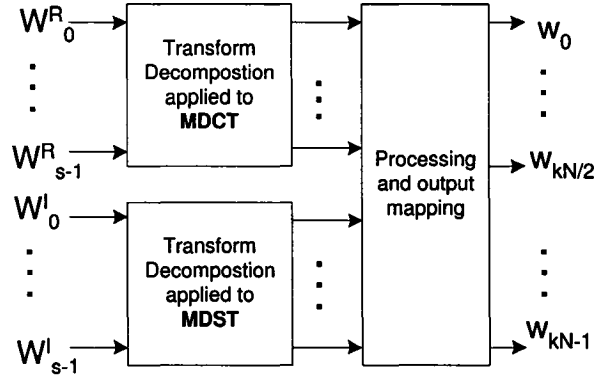
Fig. 4.3 IFFT for the non-zero taps.

such that $kN/2 = PQ$ and find the following new indices:

$$n = Pn_1 + n_2 \qquad \begin{matrix} n_1 = 0, 1, ..., Q-1 \\ n_2 = 0, 1, ..., P-1 \end{matrix} \qquad (4.43)$$

and

$$m = m_1 + Qm_2 \qquad \begin{matrix} m_1 = 0, 1, ..., Q-1 \\ m_2 = 0, 1, ..., P-1. \end{matrix} \qquad (4.44)$$

We can insert these new indices into (4.42) and we obtain:

$$MDCT(m_1, m_2) = \sum_{n_2=0}^{P-1} \sum_{n_1=0}^{Q-1} W_{Pn_1+n_2}^{R} C_{kN}^{(Pn_1+n_2)(m_1+Qm_2)}. \qquad (4.45)$$

Using trigonometrical identities, we can simplify the above equation to

$$MDCT(m) = \sum_{n_2=0}^{P-1}\sum_{n_1=0}^{Q-1} W^R_{Pn_1+n_2} \left(C_{kN}^{(Pn_1+n_2)m_1} C_{kN}^{Qn_2m_2}(-1)^{n_1m_2} - S_{kN}^{(Pn_1+n_2)m_1} S_{kN}^{Qn_2m_2}(-1)^{n_1m_2} \right)$$

$$(4.46)$$

$$= \sum_{n_2=0}^{P-1} \left(\sum_{n_1=0}^{Q-1} W^R_{Pn_1+n_2} C_{kN}^{(Pn_1+n_2)m_1}(-1)^{n_1m_2} \right) C_{kN}^{Qn_2m_2}$$

$$- \sum_{n_2=0}^{P-1} \left(\sum_{n_1=0}^{Q-1} W^R_{Pn_1+n_2} S_{kN}^{(Pn_1+n_2)m_1}(-1)^{n_1m_2} \right) S_{kN}^{Qn_2m_2} \qquad (4.47)$$

$$= \sum_{n_2=0}^{P-1} W^{RC} C_{kN}^{Qn_2m_2} - \sum_{n_2=0}^{P-1} W^{RS} S_{kN}^{Qn_2m_2} \qquad (4.48)$$

where

$$W^{RC} \triangleq \sum_{n_1=0}^{Q-1} W^R_{Pn_1+n_2} C_{kN}^{(Pn_1+n_2)m_1}(-1)^{n_1m_2}, \qquad (4.49)$$

$$W^{RS} \triangleq \sum_{n_1=0}^{Q-1} W^R_{Pn_1+n_2} S_{kN}^{(Pn_1+n_2)m_1}(-1)^{n_1m_2} \qquad (4.50)$$

If $s \leq P$, then, $n_1 = 0$ is the only possible value for n_1 in order to have non-zero results for W^{RC} and W^{RS}. We can then simplify (4.48) to

$$MDCT(m_1, m_2) = \sum_{n_2=0}^{P-1} W^R_{n_2} C_{kN}^{n_2m_1} C_{2P}^{n_2m_2} - \sum_{n_2=0}^{P-1} W^R_{n_2} S_{kN}^{n_2m_1} S_{2P}^{n_2m_2}. \qquad (4.51)$$

Similarly, the same set of operations can be applied on the MDST and we get:

$$MDST(m_1, m_2) = \sum_{n_2=0}^{P-1} W^I_{n_2} S_{kN}^{n_2m_1} C_{2P}^{n_2m_2} + \sum_{n_2=0}^{P-1} W^I_{n_2} C_{kN}^{n_2m_1} S_{2P}^{n_2m_2}. \qquad (4.52)$$

We can then sum together the MDCT and the MDST expressions, i.e. (4.51) and (4.52),

and we obtain

$$w(m_1, m_2) = 2\left[MDCT(m_1, m_2) + MDST(m_1, m_2)\right] \tag{4.53}$$

$$= \sum_{n_2=0}^{P-1} \left(W_{n_2}^R C_{kN}^{n_2 m_1} + W_{n_2}^I S_{kN}^{n_2 m_1}\right) C_{2P}^{n_2 m_2} + \sum_{n_2=0}^{P-1} \left(W_{n_2}^I C_{kN}^{n_2 m_1} - W_{n_2}^R S_{kN}^{n_2 m_1}\right) S_{2P}^{n_2 m_2}.$$

$$\tag{4.54}$$

We can deduce from the analysis of the last equation that for a fixed m_1 value, the equation corresponds to a P-point MDCT added to a P-point MDST. Therefore, given that $m_1 = 0, 1, ..., Q - 1$, it follows that we have Q P-point MDCTs added with Q P-point MDSTs. The operations regarding the new IFFT scheme are illustrated in Figure 4.4.
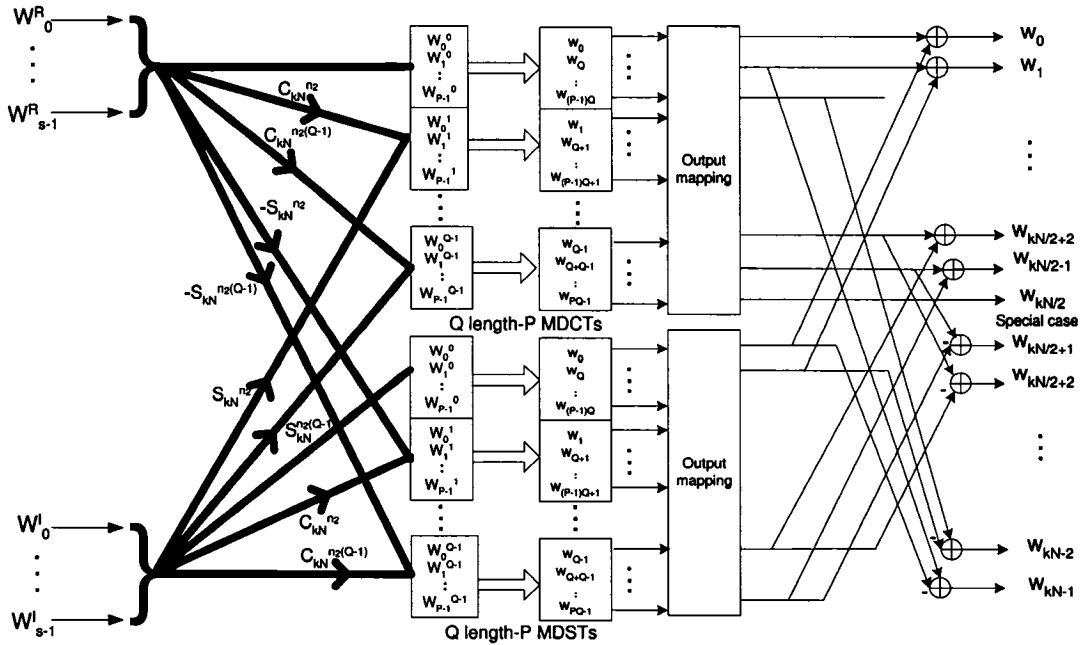

Fig. 4.4 Transform decomposition applied to a MDCT and MDST.

A comparison between the computational complexity of 512-points IFFT for three different schemes is shown on Figure 4.5. The "Transform decomposition" curve represents the application of [8] on our vector W. Indeed, it is possible to apply this algorithm by

zeroing the second half of the vector W which normally is composed of the complex conjugate symmetry of the first half. By doing so, the result of the IFFT obtained will have a redundant complex part that we can ignore while the real result part will be as if the IFFT was performed on the normal vector W. The "MDCT-MDST method" consists in the straight forward application of [9]. Finally, the "Combined method" represent computational complexity of our proposed IFFT. As it can be observed, the new IFFT scheme has the best efficiency when the ratio of non-zero taps over the IFFT length is inferior to 1/8.
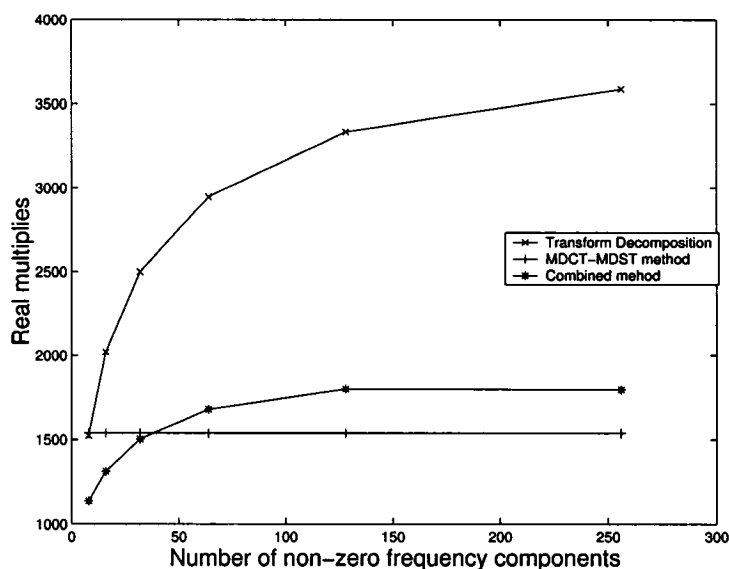
Fig. 4.5 Comparison of computational complexity for a 512-points IFFT.

4.3 Computational complexity analysis

This section analyzes in details the EC computational complexity in terms of real multiply operations. The EC of the remote terminal side is analyzed for the structure presented in [6] and for the proposed scheme with reduced complexity. The section is divided into three subsections: the first one addresses the adaptation, the second one deals with emulation, and the final one summarizes the results.

4.3.1 Adaptation

The adaptation processing part is represented by the dashed boxes on the echo canceller of figure 4.6. The adaptation processing can be divided into three parts:

- the adaptation of the echo channel coefficients in the FEC (equation(3.50)),
- the division of the frequency-domain residual echo signal by the FEQ coefficients,
- the IFFT of the frequency echo channel estimate.
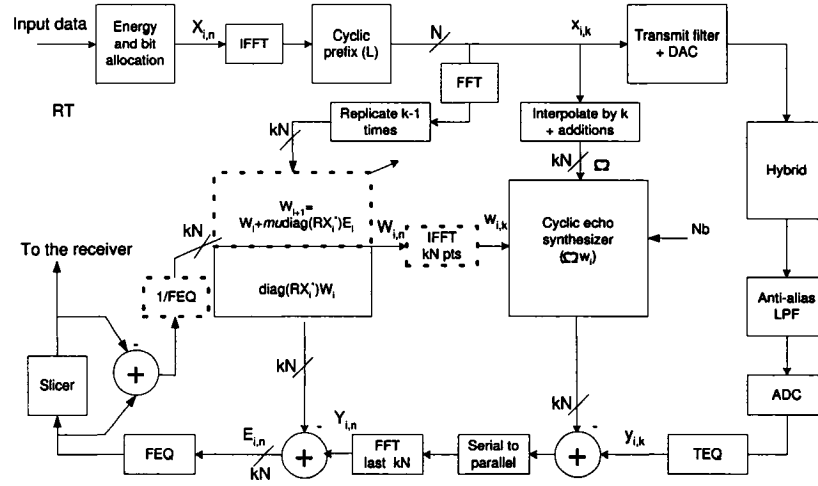
Fig. 4.6   Echo canceller at RT with the adaptation part highlighted.

In the following, we will first do the complexity analysis for the structure in [6], and then, we will use it to derive the computational complexity of the new proposed structure.

Echo canceller structure elaborated by Ysebaert [6]

Let us start with the analysis of equation (3.50) giving the adaptation of the echo channel coefficients for scheme [6]:

$$W_{i+1} = W_i + \mu\text{diag}(RX_i^*)E_i.$$

The vector E_i has $kN/2$ elements and is composed of complex numbers. The diagonal matrix $\text{diag}(RX_i^*)$ is also complex, hence the multiplication with E_i requires $kN/2$ complex multiplies. Given that one complex multiply translates into four real multiplies, we thus have $2kN$ real multiplies. The scalar μ is real, therefore we have $kN/2$ multiplications of

one real number by a complex number. For each of these, two real multiplies are required, thus equation (3.50) requires $3kN$ real multiplies.

Regarding the division of the frequency residual echo signal by the FEQ coefficients (see Figure 4.6). There are $kN/2$ complex coefficients divided by $kN/2$ complex coefficients. Therefore, a total of $2kN$ real multiplies are required to perform the division [2].

As for the computational complexity of the IFFT, it depends on the scheme to be used. In [6], the authors used the IFFT algorithm for real time-domain data described in [10]. It consists in rearranging the data in order that only a length $kN/2$ radix 2 IFFT is required with additional $kN/2$ complex multiplies. The number of real multiplies is therefore equal to $kN(\log_2 \frac{kN}{2} + 2)$. In short, for the entire adaptation part of the structure described in [6], we have $5kN + kN(\log_2 \frac{kN}{2} + 2)$ real multiply operations.

Echo canceller with reduced complexity structure

Now, in regards of our new proposed scheme, the first difference consists in the fact that solely s coefficients are adapted instead of $kN/2$. Hence, for the division of the residual echo signal by the FEQ coefficients, $6s$ real multiplies are required. Following the same reasoning for equation (3.50), solely $4s$ multiply operations are required. Thus we have $10s$ multiply operations yet to be performed plus the IFFT. In [9], it is stated that the number of multiply operations needed to perform a N-points MDCT (as well as a N-points MDST) is $\frac{N}{2} \log_2 N - N + 1$. It follows that applying exactly the IFFT scheme described in [9] needs $\frac{kN}{2} \log_2 \frac{kN}{2} - kN + 2$ real multiplies. In the previous section, another structure for the IFFT was presented. The new structure requires Q length-P MDCT and Q length-P MDST. Furthermore, the structure necessitates the multiplication of the non-zero coefficients by $4s(Q-1)$ real coefficients. The overall complexity for the new IFFT scheme is $2Q(\frac{P}{2} \log_2 P - P + 1) + 4s(Q - 1)$. In our proposed EC scheme the choice of the IFFT algorithm to be used (between [9] and the one presented in previous section) depends on the ratio of the non-zero coefficients over the length of the IFFT. Indeed, the new IFFT method becomes less effective than [9] when the ratio is higher than $1/8$. Consequently, the computational complexity of the adaptation part for the new scheme is $[10s + \frac{kN}{2} \log_2 \frac{kN}{2} - kN + 2]$ when

---

[2]In a fixed-point implementation, a division requires more computational operations than a multiplication. However, given that the FEQ coefficients can be considered as invariant in time, it is possible to calculate the inverse of the FEQ components once, and then, to use these coefficients to perform multiplication instead of division.

IFFT of [9] is used, and $[10s + 2Q(\frac{P}{2} \log_2 P - P + 1) + 4s(Q - 1)]$ when the new IFFT scheme is used.

4.3.2 Emulation

The emulation part of the EC corresponds to the operations required to create the estimated echo signal. Figure 4.7 highlights in dash line the various processing part involved in emulation. Following the same structure as in the previous subsection, we will first do the
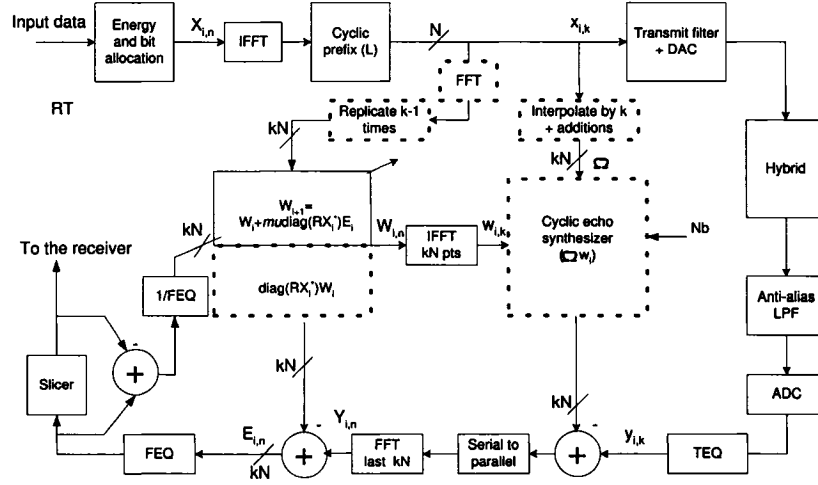
Fig. 4.7 Echo canceller at RT with the emulation part highlighted.

complexity analysis for the structure in [6], then we will use it to derive the computational complexity of the new proposed structure.

Echo canceller structure elaborated by Ysebaert [6]

For a symbol i, the emulation operations are resumed by the following equation coming from (3.49)

$$A_i = \text{diag}(R\tilde{X}_i)W_i + F_N(\tilde{\Omega}_{i-1,i,i+1}w_i) \qquad (4.55)$$

The first part of the equation $(\text{diag}(R\tilde{X}_i)W_i)$ is composed of frequency-domain signals and thus is performed by the FEC. It consists $kN/2$ complex numbers multiplied by $kN/2$ complex numbers. It follows that $2kN$ real multiplies are required for this portion of the

emulation. As it is mentioned in chapter III, the timing between the near-end and far-end signal is adjusted in order to have a proper alignment at the CO. Hence to minimize the complexity of the EC, the alignment needs to be readjusted at the RT. This is achieved by doing a FFT on the near-end signal. The complexity of a FFT for real signal is $N(\log_2 \frac{N}{2} + 2)$.

The remaining part of (4.55), i.e. $\tilde{\Omega}_{i-1,i,i+1} w_i$ is performed by the time-domain canceller. The transformation in frequency, noted by F_N is not included in the complexity calculation since it is required by the receiver whether or not the EC is present. Since the operations are performed in time-domain, all the signals are real. The matrix $\tilde{\Omega}_{i-1,i,i+1}$ is of the same form as in Figure 3.5. In the case of optimal alignment, the non-zero elements comprised in each corner of the matrix happen to be symmetrical; thus by combining the non-zero elements together, we obtain a squared matrix. Given that the length of the echo channel is known and denoted by M, we can calculate the number of non-zero values. Indeed, as shown on Figure 4.8, the number of non-zero elements is $(\frac{M-1}{2})(\frac{M}{2}) \simeq \frac{M^2}{4}$. However, because the

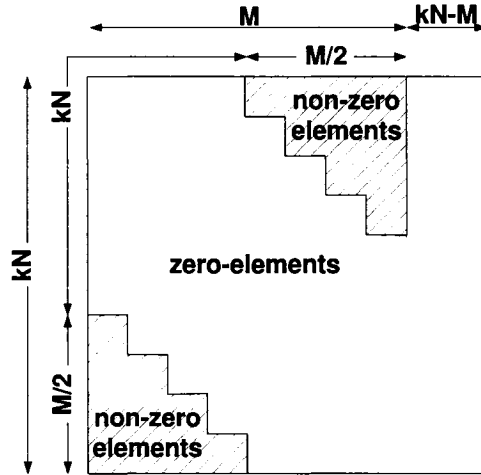

Fig. 4.8   Explanation of non-zero elements in $\tilde{\sigma}_{i-1,i,i+1}$.

non-zero elements correspond in fact to the interpolated near-end signal, only one out of k elements is non-zero. Therefore, the number of multiplies for the time-domain portion is $\frac{M^2}{4k}$. The total computational complexity for the emulation part is $2kN + N(\log_2 \frac{N}{2} + 2) + \frac{M^2}{4k}$.

Echo canceller with reduced complexity structure

From the previous calculations, we can derive the emulation complexity for our proposed EC scheme. The only difference resides in the operations realized in the FEC, i.e. $\text{diag}(R\tilde{X}_i)W_i$. Solely s complex multiplications are required due to the zeroing of the high frequency components. The computational complexity of the emulation part for our proposed scheme is $4s + N(\log_2 \frac{N}{2} + 2) + \frac{M^2}{4k}$.

4.3.3 Computational complexity summary

The results of the previous computational complexity EC algorithms for both the adaptation and emulation part are summarized in Table 4.1.

Table 4.1 Computational complexity.

	Echo canceller of Ysebaert [6]	Echo canceller with reduced complexity
Emul.	$\frac{M^2}{4k} + 2kN + N(\log_2 \frac{N}{2} + 2)$	$\frac{M^2}{4k} + 4s + N(\log_2 \frac{N}{2} + 2)$
Adapt.	$5kN + kN(\log_2 \frac{kN}{2} + 2)$	$10s + \frac{kN}{2}\log_2 \frac{kN}{2} - kN + 2$ or $10s + 2Q(\frac{P}{2}\log_2 P - P + 1) + 4s(Q - 1)$

Chapter 5

Results and discussions

The aim of this chapter is to validate the innovations described previously in chapter 4. This is achieved by accomplishing computer simulations on a DSL modem simulator built with the use of Matlab software. The present chapter is divided as follows. The first section describes the characteristics of the simulator. The second section is devoted to the validation of the simulator. The performance of our proposed techniques is demonstrated in the third section. The latter section also illustrates the computational complexity reduction achieved by the proposed EC algorithm simplifications in comparison with optimal EC of [6].

5.1 Characteristics of the modem and methodology

The simulator is built to model the reception of an ADSL-like communication at the RT modem. In ADSL, the frequency bandwidth of the signal transmitted by the RT modem is eight times ($k = 8$) smaller than the frequency bandwidth of the signal received. Figure 3.8 illustrates the various processing blocks of the modem that is recreated in our simulator. The simulator has the following fundamental ADSL characteristics:

- the frequency bandwidth of a tone is 4.3125 kHz,
- 32 tones are used in upstream (64-point FFT),
- 256 tones are used in downstream (512-point FFT),
- the sampling frequency of the RT receiver is 2.208 MHz,
- the sampling frequency of the RT transmitter is 276 kHz,
- a cyclic prefix of 5 samples is used in upstream,

- a cyclic prefix of 40 samples is used in downstream,

- the length of a received frame at the RT side is 552 time-domain samples,

- the transmit signal power is -40dBm/Hz in upstream and downstream,

- the length of the TEQ is 32,

To simplify the elaboration of the simulator, 4-QAM is used in every tone to transmit data. Transmitting subsymbols with only 4-QAM constellation does not affect the validity of our simulation. The reason is that the output of the simulations corresponds to the squared difference between the frequency representation (constellation point) of the far-end signal and the received signal (MSE or SE). As long as the proper subsymbol is decoded, the simulation results between a simulator using 4-QAM and multi-QAM will be similar.

NEXT interference signal is added to the received signal coming from the far-end (CO). The NEXT introduced corresponds to the presence of 10 ADSL interferers and is calculated according to equation (2.3). The Additive White Gaussian Noise (AWGN) signal level is set to -140 dBm/Hz. No FEXT interference signal is added. The echo channel impulse response used in the simulator is illustrated on Figure 5.1. The transfer function of the channel is based on the hybrid impedance analysis described in [12]. Visually, the echo channel impulse response of Figure 5.1 is very similar to the measured echo impulse response shown in [23]. The echo channel function depends on the wire loop composition between the RT and the CO. Thus, for the purpose of our simulations, the carrier serving area (CSA) loop #1 illustrated on Figure 5.2 is used. The loop is composed of different segments in which either a different wire is used or a bridge tap is inserted. The numbers following the "#" sign in Figure 5.2 represents the American Wire Gauge (AWG) number and the numbers below that represent the length of the wire sections. According to a field survey data [12], this loop form is very common.

The front-end receiver filter as well as the filter involved in the DAC are modelled as Butterworth lowpass filter with corner frequency of, respectively, 1.104 MHz and 138 kHz. The TEQ coefficients are taken from a Matlab Toolbox [24] in which the maximum geometric SNR method [14] is used. To focus on the performance of the EC, imperfections due to the TEQ and FEQ are removed during the processing of the signals of interest.

Figure 5.3 illustrates the frequency response of the various channels in which the near-end signal is going through, thus, creating the echo interference signal. As it can be observed, the magnitude of the near-end signal decays rapidly after the cutoff frequency (138kHz/1.104MHz = 0.39 rad/sample).
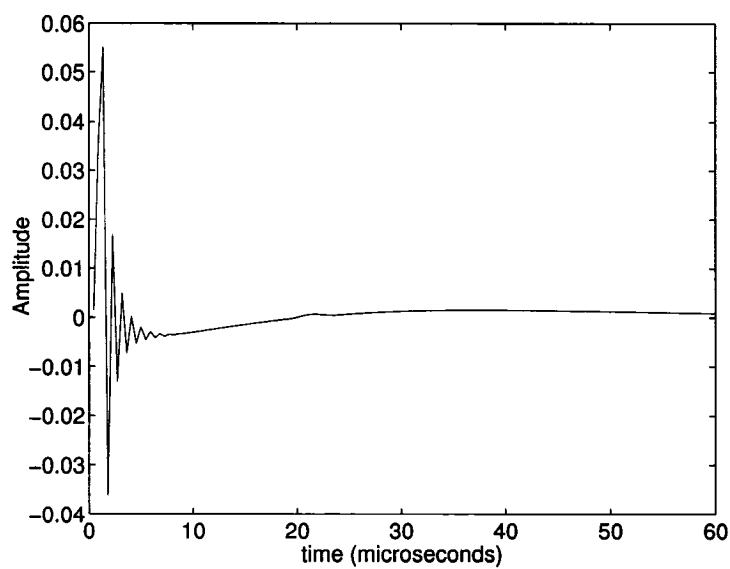
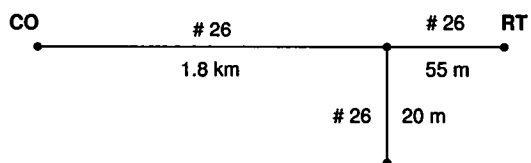**Fig. 5.1**   Echo channel impulse response.

Fig. 5.2   Composition of the loop.

As mentioned previously, the channel estimated by the echo canceller is the channel corresponding to the joint effects of the DAC low pass filter, the imperfect hybrid and the TEQ. The time-domain impulse response of this channel is illustrated on Figure 5.4, while its frequency-domain magnitude response can be found on Figure 5.3. In the upcoming simulation results, the number of time-domain taps used for the echo channel estimate is 300 which corresponds to $136\mu s$. As it will be proven in the next section, the time-domain tap above 300 can be considered as negligible for the purpose of our simulations.
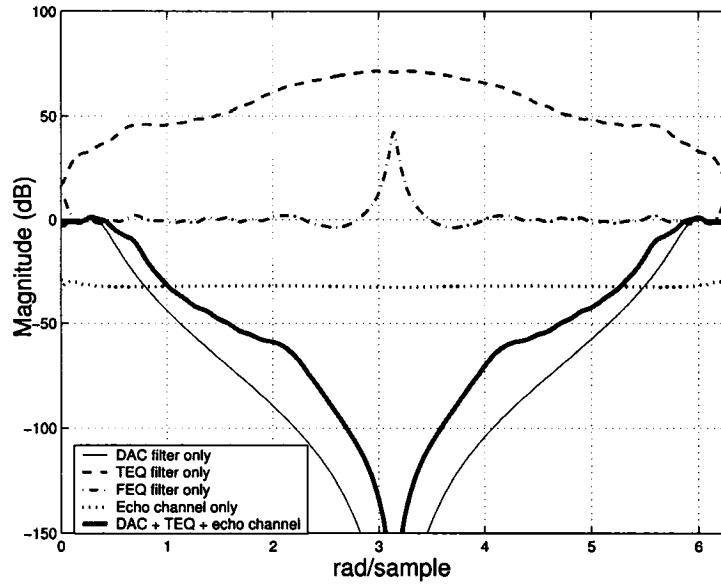

Fig. 5.3 Frequency-domain magnitude responses of the various channels present in echo cancellation.

To verify the performance of the proposed EC, three different metrics will be used. The first one expresses the frequency-domain mean square error (MSE) of the echo cancelled signal after each iteration. More precisely, for iteration i, this is defined as :

$$MSE_i = \frac{1}{257} \sum_{n=0}^{256} 10\log_{10}|E_{i,n}|^2. \tag{5.1}$$

where $E_{i,n}$ refers to a single element of the vector defined by (3.49). Evaluating the MSE by using the dB value of the tones instead of the linear value avoids the eventuality that a big error on a particular tone masks the remaining error values on the other tones. Therefore,
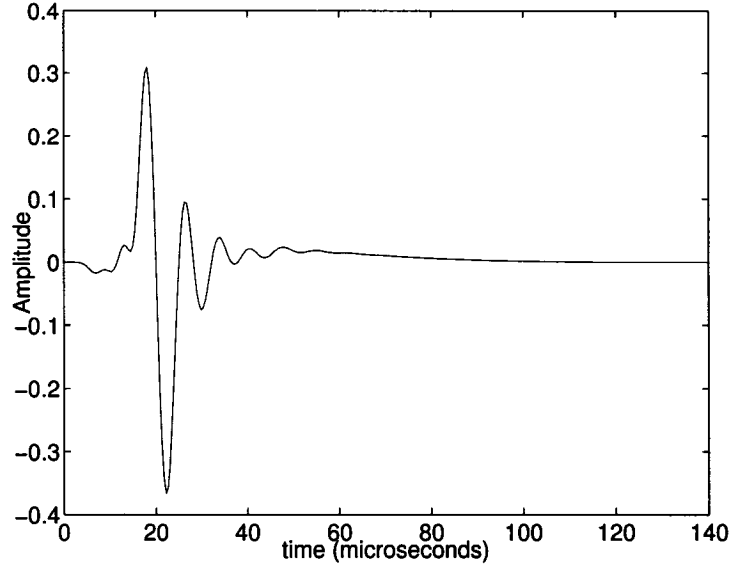
Fig. 5.4 Echo channel impulse response as seen by the EC (ADC, imperfect hybrid, and TEQ).

this MSE metric gives a better idea of the EC on all the tones. One should note that 257 tones are used (not 256) in the evaluation of the MSE due to the special configuration that real time-domain sequences exhibit in their FFT representations.

The second metric used for evaluating the performance of the EC consists in averaging the frequency-domain squared error of the echo cancelled signal over several iterations for each tone:

$$\overline{SE}_n = \frac{1}{P} \sum_{i=Z}^{Z+P} 10\log_{10}|E_{i,n}|^2, \tag{5.2}$$

where Z is the iteration number at which we can establish that the EC has converged, and P corresponds to the number of iterations over which the average is calculated. In fact, if we add $10\log_{10}(512 \times 0.001\text{Watt} \times 1.104\text{MHz})$, i.e. -57.5 dB, to $\overline{SE}_n$ we get a form of power spectral density estimate of the error, expressed in dBm/Hz units.

The third and last metric used is the power of the frequency-domain error $E_{i,n}$ that we

expressed as[1]

$$P_i = \frac{1}{512^2} \sum_{n=0}^{511} |E_{i,n}|^2.$$ (5.3)

The above measures will be used to evaluate the performance of the adaptive EC, in both terms of:

- convergence speed,

- average echo loss after steady-state initial convergence.

The LMS step size used in the echo canceller is set to 0.1.

5.2 Validation of the simulator

The validation of the simulator is realized through three special simulation cases. Each of them validates different parts of the simulator, as described below.

5.2.1 Validation of the noise signal and power

The first set of simulations is intended to validate the AWGN and NEXT signals implemented in the simulator. Therefore two simulations are required; one for AWGN and one for NEXT. The first simulation is performed under the following conditions:

- strictly AWGN noise environment,

- no echo interference in the system,

- perfect propagation channel impulse response, i.e. no degradation of the far-end signal, no TEQ and no FEQ.

Figure 5.5 shows the performance of the system in such conditions. As it can be seen, the MSE_i as well as the $\overline{SE_n}^2$ oscillate around -82dB. This value comes from the AWGN and can be explained as follow. Let c_n represents one element of the FFT noise signal, thus given that the frequency error on a tone is in fact the noise, we should have in theory $|c_n| = |E_{i,n}|$. Moreover, given that the noise is white, the mean of the error on each tone

---

[1] According to Parseval's relation for the DFT, the total energy contained in the frequency sampling is given by $\varepsilon = \frac{1}{N} \sum_{n=0}^{N-1} |E_{i,n}|^2$, thus the average power is obtained as $\frac{\varepsilon}{N}$, as given by (5.3) where $N = 512$.

[2] The value of P used in (5.2) is 200.

is the same, in other words the expected value of $|E_{i,n}|$ is the same for any combination of $\{i, n\}$. We know that the power of the AWGN is equal to

$$P_{AWGN} = 10\log_{10}\left(\frac{\frac{1}{512^2}\sum_{n=0}^{511}|c_n|^2}{0.001\text{Watt} \cdot 1.104\text{MHz}} \right) \tag{5.4}$$

$$= 10\log_{10}\left(\frac{\frac{1}{512^2}\sum_{n=0}^{511}|E_{i,n}|^2}{0.001\text{Watt} \cdot 1.104\text{MHz}} \right) = -140\text{dBm/Hz}. \tag{5.5}$$

Thus, it is possible to isolate $|E_{i,n}|$ from (5.5), to put this number back into (5.1) and (5.2), and we get a theoretical value of -82.5 dB for both the MSE_i and the $\overline{SE_n}$, which is very similar as the results on Figure 5.5. This simulation validates the noise signal interference as well as the MSE_i and $\overline{SE_n}$ measurements.
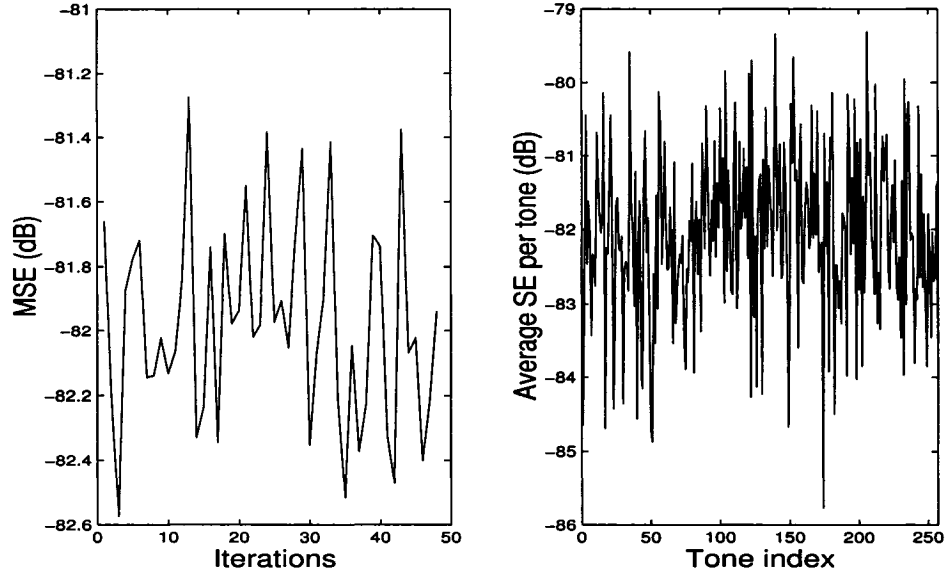

Fig. 5.5 MSE_i and $\overline{SE_n}$ performance in AWGN environment without echo interference and with perfect propagation channel.

We can use a similar procedure to validate the performance of the simulation in the presence of NEXT. Instead of running the simulation with AWGN only, the simulation is ran with NEXT interference only. In this case, however, the MSE_i curve is of no use since the NEXT varies in frequency. Therefore, as shown on Figure 5.6, only the $\overline{SE_n}$ is calculated. If we subtract -57.5 dB on every point of the curve, we get a PSD estimate (in

dBm/Hz) of the NEXT signal as mentioned in previous subsection. We can verify that the NEXT PSD figure obtained in this way is very similar to that shows in [18] for the same combination of 10 ADSL disturbers.
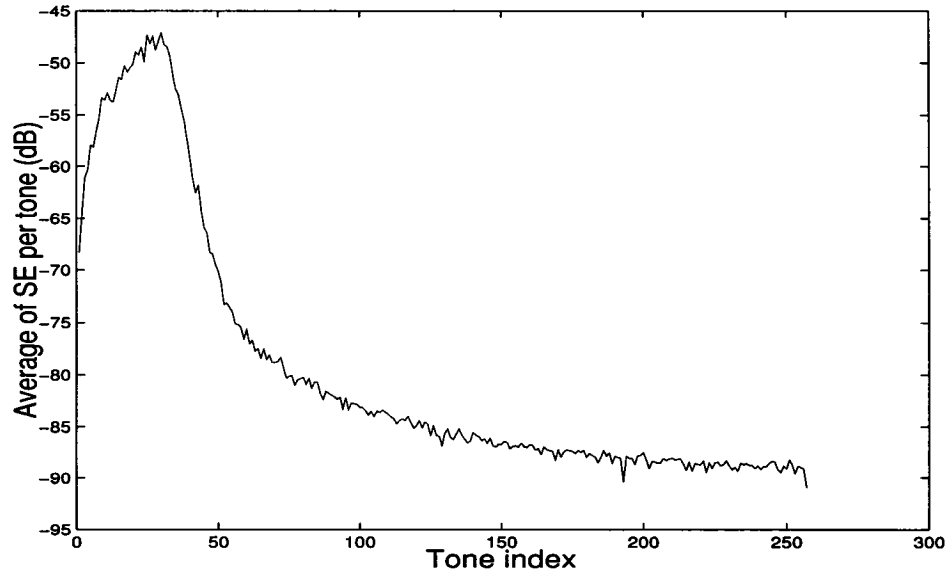

Fig. 5.6 $\overline{SE_n}$ performance in NEXT environment without echo interference and with perfect propagation channel.

5.2.2 Validation of the TEQ and FEQ

The aim of this second set of simulations is to validate the processing related to the propagation channel, i.e. the combination of the TEQ with the FEQ. In order to achieve this, a simulation is run under the following conditions:

- with propagation channel activated,

- no echo interference,

- noise free environment.

The experimental MSE_i resulting from such simulation corresponds to -300dB (i.e. machine precision), which means that the signal decoded at the receiver matches perfectly the far-end transmit signal. Thus the TEQ and FEQ are set properly for the corresponding propagation channel.

5.2.3 Validation of the echo canceller algorithm

Finally, the third validation case aims to verify that our implementation of the adaptive echo cancellation scheme [6] works properly. This is achieved by using the simulator under the following conditions:

- with propagation channel activated,

- with the presence of echo interference,

- noise-free environment.

We should notice a constant diminution of the residual echo interference as the iteration number increases. Figure 5.7 illustrates simulations in which the residual echo power P_i is plotted for two different numbers of time-domain taps used in the echo channel estimate. As it can be observed, P_i saturates around -130dB for a length of 300 taps. When we increase the number of taps to 325, the power of the residual echo signal saturates around -147dB and the convergence speed is a little slower. This behavior is due to the fact that part of the echo channel impulse response is composed from the Butterworth lowpass filter included in the DAC. Given that this filter is an IIR filter, the echo channel impulse response is also IIR, and thus, it is of infinite length. Therefore, the convergence of P_i occurs at a lower level when we increase the number of time-domain taps. This behavior is qualitatively consistent with the results reported in [6]. We can thus state that our implementation of the echo canceller algorithm works properly.

5.3 Results

The following section is divided into two parts, the first part is devoted to the performance of the fast initialization technique and the second part illustrates the performance of the reduced complexity echo canceller.

5.3.1 Fast initialization technique

In this subsection, we will first begin by verifying the theoretical approximation (chapter 4.1) of the residual echo signal power left in the system after applying the fast initialization technique. By doing so, we will also quantify the performance of the technique in terms of
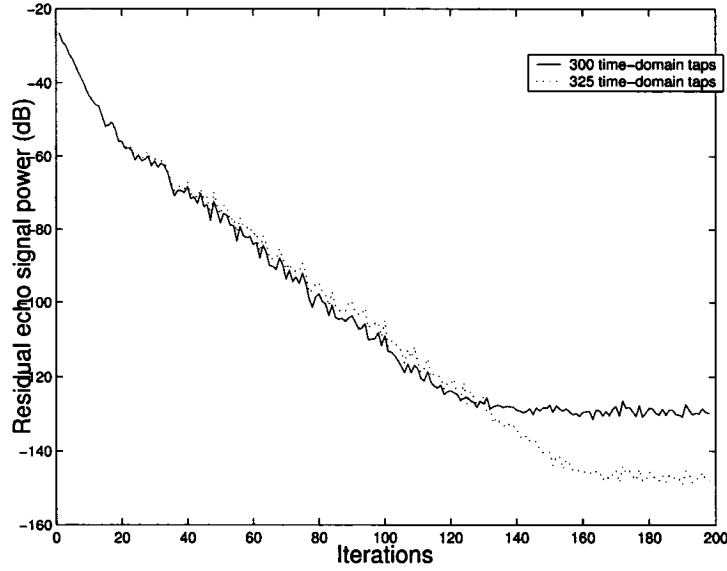
Fig. 5.7 Residual echo power in noise-free environment and usual propagation channel.

number of LMS iterations saved in comparison with simulation ran without the use of the fast initialization technique. The second part of this subsection will present the same set of results in a real environment where AWGN and NEXT are present.

Given that the theoretical derivation of the residual echo power in (4.26) assumes that echo is the only interference signal in the system, the different sets of simulations will be run in noise-free environment. Figures 5.8 to 5.12 compare the average power of the residual echo signal in the system for 100 simulations using fast initialization technique with that of 100 simulations using solely standard LMS algorithm [6], i.e. initializing the EC frequency-domain taps to zero. Five different misalignment values were used ($\Delta \in \{0, 30, 40, 60, 80\}$) and the step size of the LMS is set to 0.1.

The fast initialization algorithm performs the best when a misalignment of 20 samples ($\Delta = 30$) occurs between the transmit and receive signals. As a matter of a fact, up to 19 LMS iterations can thus be saved in comparison as without the use of the fast initialization algorithm. This improvement translates into a speed up of 19x552samples/2.208MHz= 4.75ms in convergence time. This optimal alignment principally depends on the shape and length of the echo channel. As it can be seen, above a misalignment of 80 samples, the fast initialization technique has little efficiency.

Figure 5.13 compares the theoretical approximation of power reduction due to the fast initialization technique, as per equation (4.36), with the experimental results. As it can be observed, on overall the theoretical approximation is fairly close to the experimental results; the error between the theoretical approximation and the experimental result is constrained between -3.8dB and 0.7dB over the range of Δ shown. For values of Δ larger than 30 samples, there is good agreement between the values predicted by formula (4.36) and the results of the simulations; for smaller values of Δ a more accurate formula could be derived by taking into account higher order terms (i.e. those obtained by taking into account $E\{C_{i,\Delta}^{-1}\Omega_{i-1,i,i+1}h\}$ in (4.32)).
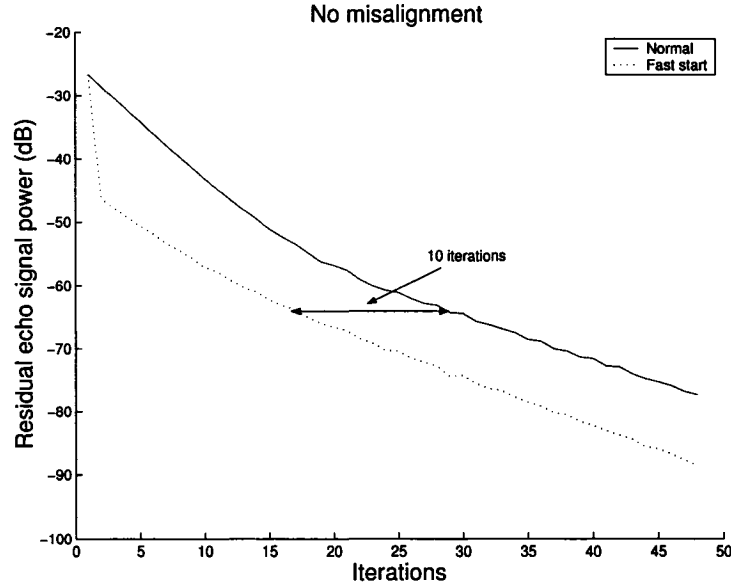

Fig. 5.8 Comparison of the residual echo signal power between fast initialization algorithm and usual algorithm for $\Delta = 0$

Figure 5.14 compares the reduction of the error signal power due to the fast initialization technique in a real environment (i.e. when NEXT and AWGN are present) for different values of misalignment. As it can be observed, the presence of the NEXT and AWGN affects the performance of the fast initialization algorithm since the maximum improvement of residual echo power due to the fast initialization technique is 11.3 dB (as shown on the figure for perfect alignment) while it is 27.7 dB in noise-free environment. In term of the

Fig. 5.9 Comparison of the residual echo signal power between fast initialization algorithm and usual algorithm for $\Delta = 30$

Fig. 5.10 Comparison of the residual echo signal power between fast initialization algorithm and usual algorithm for $\Delta = 40$
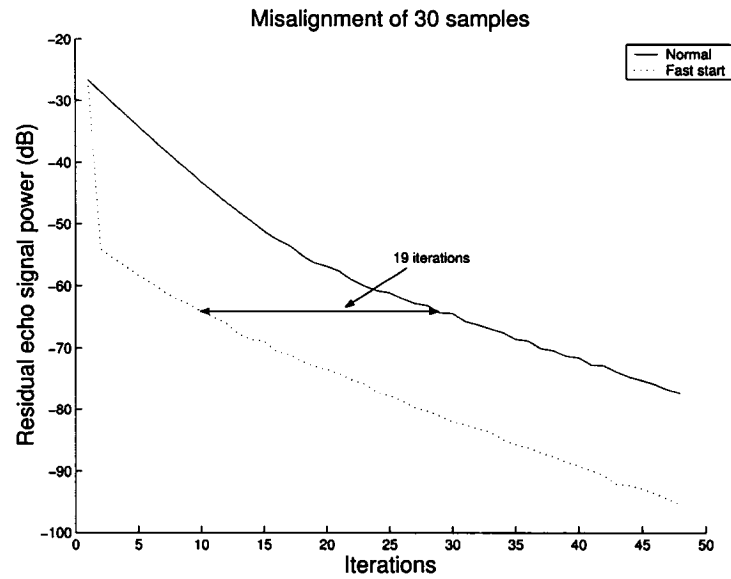
Fig. 5.11   Comparison of the residual echo signal power between fast initialization algorithm and usual algorithm for $\Delta = 60$
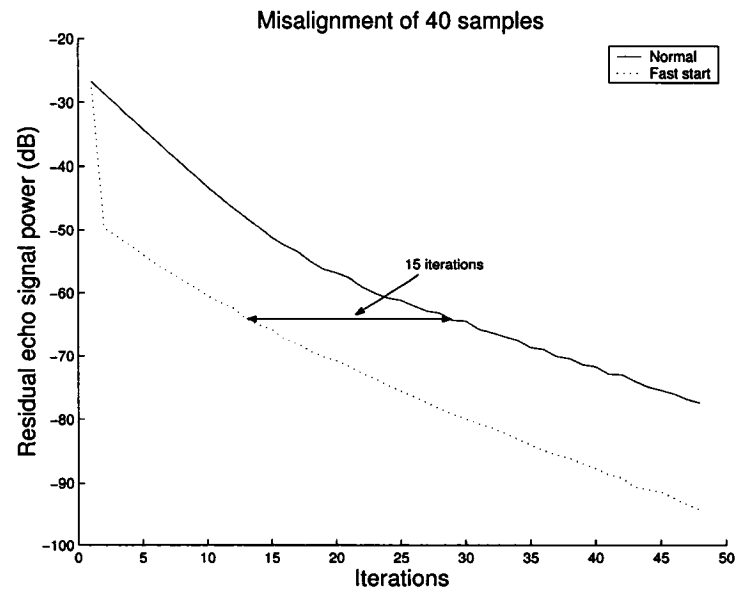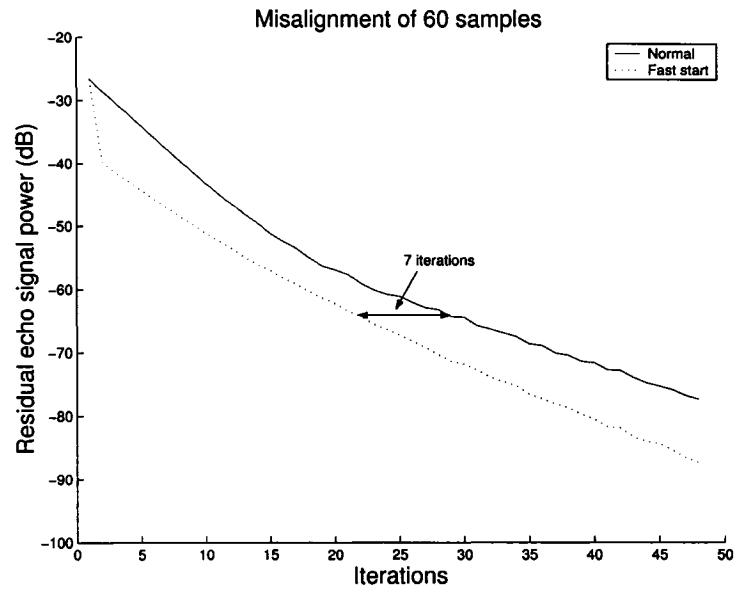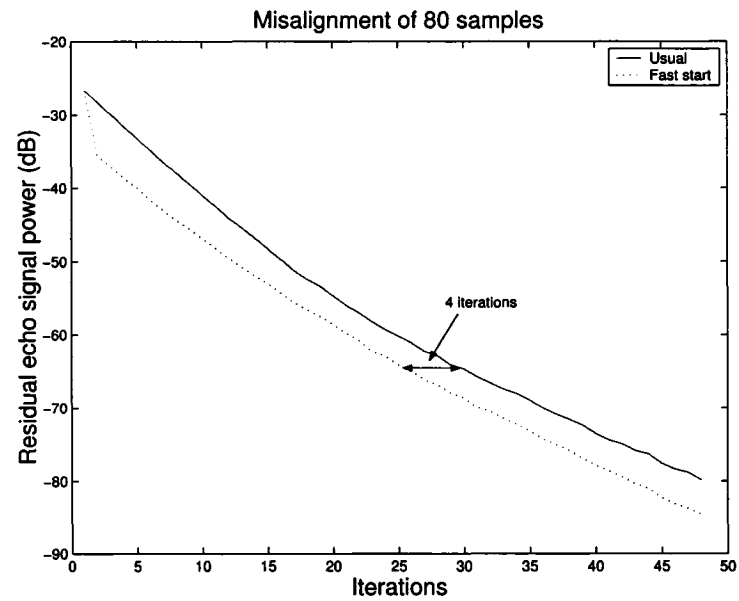

Fig. 5.12   Comparison of the residual echo signal power between fast initialization algorithm and usual algorithm for $\Delta = 80$
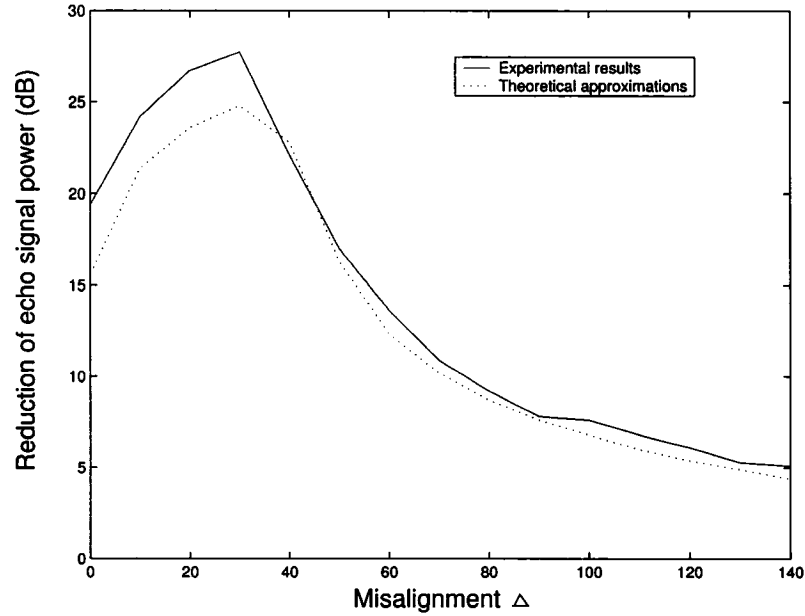
Fig. 5.13 Comparison of the residual echo signal power due to initialization technique between theoretical approximation and simulation results.

maximum number of LMS iterations saved by the technique, the graphic demonstrates that around eight to ten iterations can be saved in real environment while it is precisely 19 in noise-free environment. This degradation of performance can be mainly attributed to the severe NEXT interference. From Figure 5.14, it can also be noticed that above a misalignment of around 80 samples, even though there is still an improvement of residual echo signal power due to the initialization technique of 6.8 dB, the number of LMS iterations required to reach the final convergence region (around -40dB) does not diminishes. We can thus state that for this particular echo channel, the fast initialization technique improves the speed for which the EC converges as long as more than 6.8 dB of residual echo power improvement is achieved by the technique.

5.3.2 Reduced complexity echo canceller at RT

The technique used to reduce the computational complexity of the EC at the RT consists in zeroing the high frequency components of the estimated echo channel. The optimal starting frequency index from which the zeroing of the components occurs depends on the
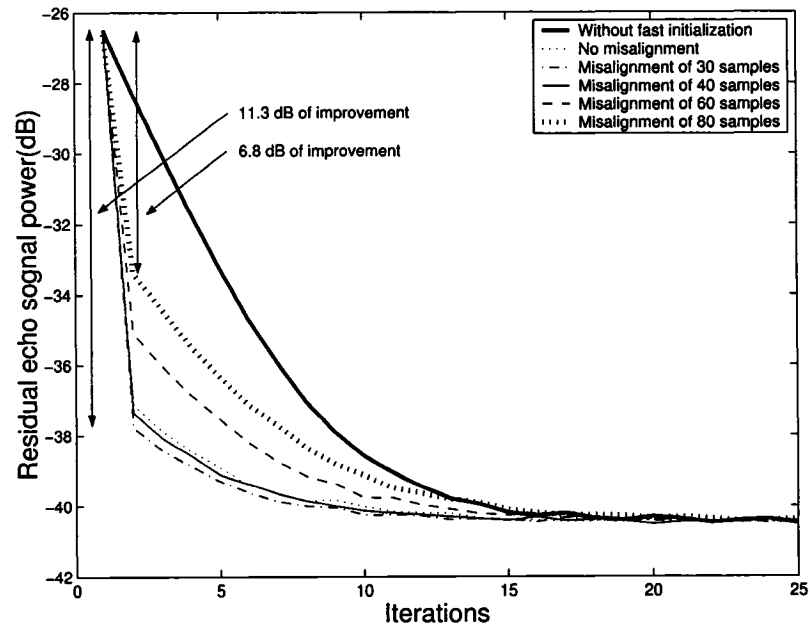
Fig. 5.14 Comparison of the residual echo signal power when the fast initialization technique is used in real environment for $\Delta = 0, 30, 40, 60, 80$.

relative echo signal magnitude level and the noise plus interference level, when expressed in the frequency-domain.

Determination of the frequency index for the zeroing technique

The best approach to determine the frequency tap number s from which the remaining taps are zeroed consists in calculating the achievable bit rate (according to equation (2.2)) for different values of s. To calculate a proper value of SNR for each tone, we averaged the received error signal ($E_{i,n}$) over 800 iterations taken after the power of the residual error had converged. The value of the gap used in equation (2.2) is 6 dB which is a very conservative value according to [18]. The objective is to maximize the bit rate while reducing as much as possible the computational complexity, therefore, the optimal s consists in choosing the smallest value of s within the maximum achievable bit rate convergence region.

Figure 5.15 and 5.16 illustrate the achievable bit rates for different values of s used in the zeroing EC technique in comparison with the achievable bit rate of [6][3]. In [25], it is mentioned that typically a fourth-order lowpass filter is used in the DAC. However, in a purpose of simplification, we enclosed the effects of the lowpass transmit filter in the DAC. Thus, Figure 5.15 uses a fifth-order filter in the DAC while Figure 5.16 uses an eight-order filter. As it can be seen, the optimal values of s are, respectively, 105 and 75 for the fifth-order and eight-order filter. These values represent the smallest value of s for which the achievable bit rate has converged[4]. The proposed zeroing EC algorithm has better performance than the algorithm in [6]. Indeed, around 35 more kbps can be transmitted with our proposed algorithm for both the fifth-order and eight-order filter. As mentioned in chapter 4, this improvement is due to the fact that zeroing the high frequency components of the echo channel represents a better estimation of the echo channel than trying to estimate the echo channel when the noise power level is higher than the echo interference power level (as in [6]).

Given that the NEXT comes from near-end signals, we used the same filter order as in the transmitter DAC to model the PSD from which the NEXT is calculated from. Therefore, the maximum achievable bit rate of the fifth-order case is lower than the eight-

---

[3]This curve is independent of the number of non-zero echo channel taps; it is shown there for the purpose of bit rate comparison.

[4]We established the beginning of the convergence region by determining the first point of the bit rate curve for which the slope is negative.

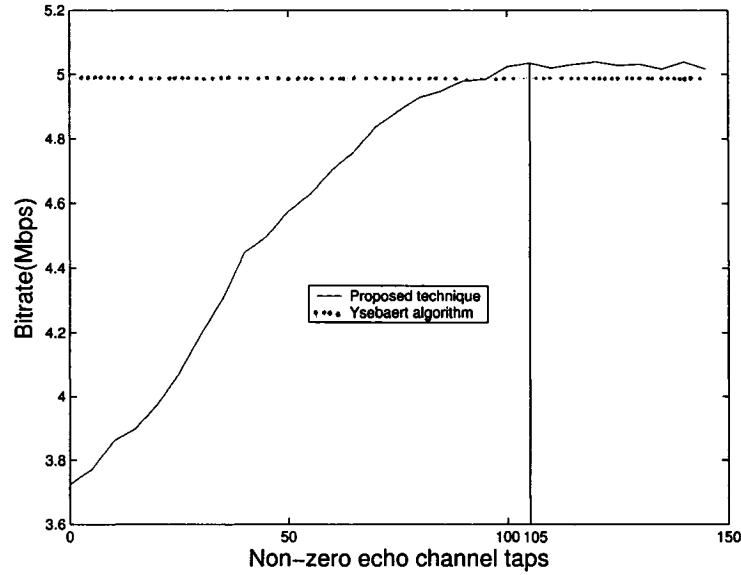order case because the NEXT has more leakage for lower order filter.

Fig. 5.15 Comparison of achievable bit rate between the zeroing EC technique and the algorithm in [6] when a fifth-order Butterworth filter is used in the DAC.

Computational complexity reduction

The principal objective pursued by the zeroing technique is to avoid the useless computational operations related to the high frequency components of the estimated echo channel.

In terms of computational complexity gain, Figure 5.17 shows the number of real multiply operations needed by our proposed scheme in comparison with that needed in [6]. In our proposed scheme, the frequency indexes from which the zeroing of the taps occurs are the same as those found in the previous section: $s = 105$ for the fifth-order filter and $s = 75$ for the eight-order filter. The complexity is plotted as a function of the number of time-domain taps used in the EC. As it can be seen, the computational complexity varies considerably as a function of the number of time-domain taps being used.

Figure 5.18 shows the computational complexity of an EC that uses 300 time-domain taps. The complexity is plotted as a function of the number of non-zero frequency echo channel taps. The EC of Ysebaert [6] is represented by a straight line since the algorithm
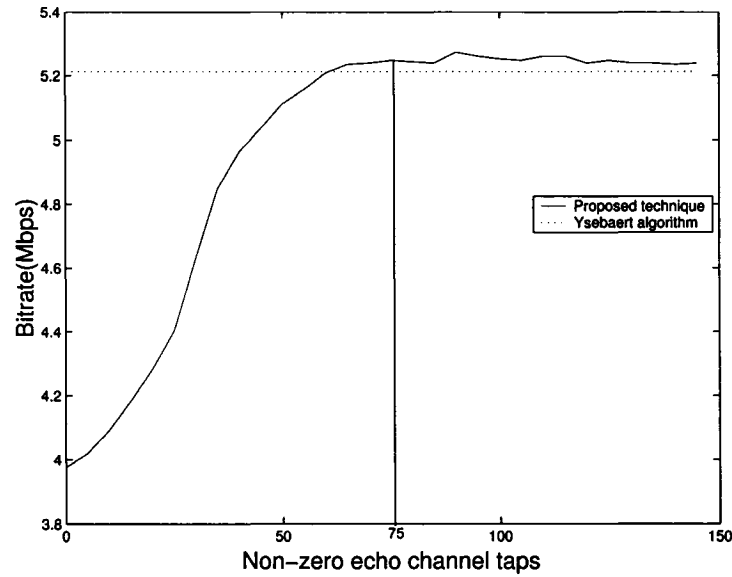
Fig. 5.16 Comparison of achievable bit rate between the zeroing EC technique and the algorithm of [6] when an eight-order Butterworth filter is used in the DAC.
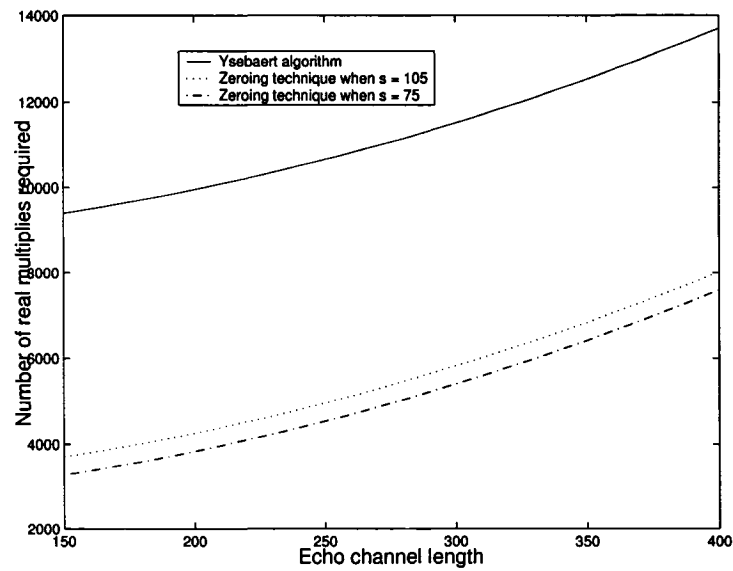

Fig. 5.17 Computational complexity of the zeroing technique in function of the number of time-domain echo channel taps.

is independent of the number of non-zero echo channel taps; this line is shown for purpose of comparison. The curve in the middle illustrates the complexity when solely avoiding the calculation of high frequency echo channel taps, while the bottom curve takes also into account the computational complexity reduction that results from the optimal choice of the IFFT algorithm. More precisely, in the case where $s \leq 32$, the new IFFT developed in section 4.2.2 has the lowest computational complexity, otherwise the IFFT of [9] is better.

For the ADSL-like configuration mentioned previously in which an eight-order Butterworth filter is used, 53% fewer multiplies are required for our proposed scheme where 22% of this saving results from zeroing the frequency taps in the FEC and 31% are due to the simplifications of the IFFT. In the case where a fifth-order Butterworth filter is used, these percentages drop respectively to 50%, 18% and 32%. One should note that in the two particular simulated cases, the IFFT of [9] represented the best IFFT scheme.
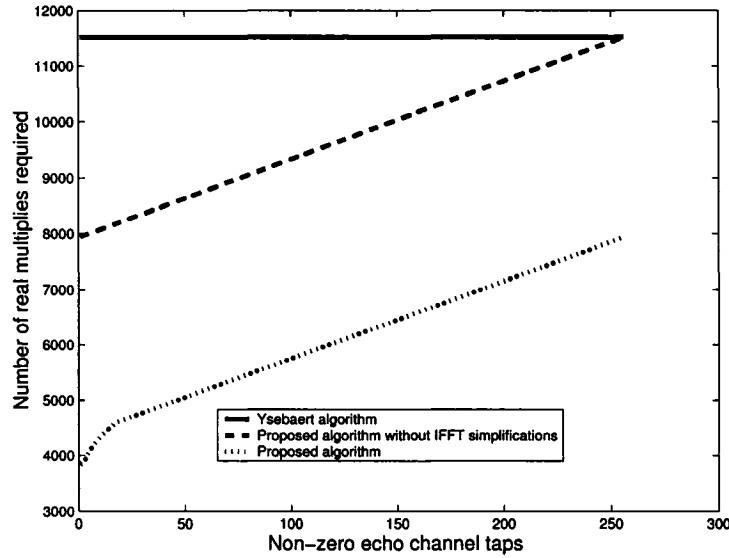
Fig. 5.18 Computational complexity of the zeroing technique versus the algorithm of [6] when 300 time-domain taps are used.

In comparison with [6], it can be concluded that the zeroing technique is more effective when the leakage coming from the imperfect DAC is smaller and when the ratio of the transmit frequency bandwidth over the receive frequency bandwidth is smaller. Indeed, these two factors contribute to increasing the number of zeroed estimated echo channel taps, which reduces the number of computational operations. A good combination of these

two factors may also allow the usage of the simplified IFFT scheme proposed in Section 4.2.2 which also has a very low computational complexity.

Chapter 6

Summary and Conclusion

Two goals were pursued through the realization of this research. The major purpose was to design an echo canceller scheme with lower computational complexity for the case of multi-rate communication, and the second goal was to increase the initial speed of convergence of the echo canceller algorithm. To fulfill these objectives, different ideas were proposed. Below, we briefly review our work and summarize its main contribution and conclusions.

In chapter Two, some fundamental aspects related to data communication in DSL environment were reviewed. The discrete multi-tone modulation (DMT) principle was presented first. Afterward, a general DMT-based DSL transceiver was presented, along with explanations on the prefix and suffix additions. Origin of the echo interference in DSL was then introduced as well as the notion of crosstalk interference. A brief overview of the characteristics of ADSL and VDSL technologies was also presented.

Chapter Three began with the description and analysis of the electric signals related to echo cancellation in DSL. These signals were then used to determine the mean square error cost function used to remove the echo interference, and to derive the least mean square equation required for updating the echo channel estimate. On this basis, a survey of the recent echo canceller algorithms was presented for symmetrical and asymmetrical rate communication in DSL.

With the help of this background material, Chapter Four presented the innovations that fulfill the purposes of the research, more precisely, a faster initial EC convergence technique and a reduced complexity echo canceller structure for the multi-rate case. Faster initial convergence is achieved by a better initialization of the frequency-domain channel

coefficients. The technique is based on the approximation of the linear convolutions involved in the system by circular convolutions. A theoretical approximation of the residual echo interference power due to the fast initialization technique was developed for the particular case of noise-free environment. The latter is made possible by considering the similarities between the power equations of the circular and linear convolutions. The efficiency of this technique was shown to be dependent on the alignment of the transmit signal from the near-end with the useful FFT block of the received signal. Further away, we then investigated how the computational complexity of the multi-rate echo canceller at the RT side described by Ysebaert *et al.* [6] could be reduced by avoiding to estimate the echo channel components corresponding to high frequencies. In effect, the frequency component index beyond which we stop to estimate the echo channel is determined by the frequency point at which the echo signal magnitude reaches the noise plus crosstalk level. Avoiding the adaptive update of these corresponding coefficients signifies that the frequency-domain echo channel representation contains many zeros, and thus, leads to simplification in the IFFT process required by the EC. In the last section of Chapter Four, we explained how it is possible to merge the pruned IFFT method developed by Sorensen *et al.* [8] with the adapted IFFT for OFDM transmission developed by Wu *et al.* [9]. The resulting IFFT technique achieves a lower computational complexity than [8] and [9] when the ratio of the number of non-zero coefficients over the IFFT length is below 1/8, which may not always be the case in DSL.

To verify the effectiveness of our proposed techniques, different experiments were conducted in a DSL simulator in which a typical ADSL environment was reproduced. Chapter Five was dedicated to the presentation of the simulation results. The first section began by explaining the diverse characteristics of the simulator. Afterward, the functionality of the simulator was verified through different sets of simulations in which different functionalities were activated or deactivated according to the characteristics to be tested. The third section showed the performance of the fast initialization technique for different timing alignments between the transmit and receive signals. Hence, it was shown that the best alignment between the transmit and receive signals occurs when the far-end signal is delayed by 40 samples in comparison with the near-end signal. As a result, with the use of the fast initialization technique in noise-free environment, the EC reaches the steady-state convergence region with 19 LMS iterations faster than when the EC is conventionally initialized to zero. The difference between the theoretical approximation of residual echo

power derived in chapter Four and the experimental results varies between -3.8dB and 0.7dB for a range of misalignment of $0 \leq \Delta \leq 140$. In a real environment, the NEXT interference affects significantly the performance of the technique such that the theoretical approximation is not valid anymore. For the optimal alignment, an improvement of only 11.3 dB of residual echo power is achieved in comparison with 27.7 dB in noise-free environment. The maximum number of LMS iterations saved in the case of perfect alignment drops to around ten. The efficiency of the technique highly depends of the misalignment; in our particular simulated case, the fast-initialization technique performs the best for a misalignment of 30 samples. The performances gradually diminishes as the misalignment changes from the optimal number of samples.

The last section of chapter five presented the performance of the reduced complexity EC technique for two different lowpass filter orders. As expected, more frequency-domain echo channel coefficients can be approximated to zero when a higher filter order is used since the echo signal magnitude expressed as a function of frequency reaches the noise floor faster. Thus, for a fifth-order and eight-order lowpass filter, respectively, 41% and 29% of the number of frequency-domain echo canceller taps used in [6] are required with our proposed method. The comparison of the bit rate curves calculated from the reduced complexity EC with the bit rate curves calculated with the EC of [6] showed that our algorithm performs a little better; about 35 more kbps can be transmitted. This improvement is due to the fact that zeroing the high frequency components of the echo channel represents a better estimation strategy when the noise power level is higher than the echo interference power level (in comparison with [6]). Finally, in terms of computational complexity, it was shown that the proposed echo canceller technique, that includes the optimal IFFT scheme, requires up to 53 % fewer multiply operations than [6] when the lowpass filter order of the DAC is eight, and 50% fewer multiplies operations when the lowpass filter is five.

We do not see any issue regarding the implementation of the two proposed techniques in a real modem. The fast initialization technique may not always be of a great help since it greatly depends on the shape of the echo channel impulse response and also of the alignment between the receive and transmit signal. Moreover, the alignment is usually fixed in order to avoid an FFT at the central office side which is most probably more important than increasing the speed of convergence. An extended study should be performed on different echo channel impulse responses to verify the variation of performance of the technique. The implementation of the reduced complexity technique is very flexible since the frequency

from which the echo channel components are approximated to zero is easily modifiable. Moreover, it is possible to establish a worst case condition in terms of interference and noise such that we know that the echo signal power will always be below the noise floor from that particular frequency index.

In this work, the reduced complexity technique was implemented on the RT modem, however, it should be noticed that the technique could also be applied on the CO modem. Indeed, at the CO side, the frequency echo canceller developed by [6] operates at high frequency to counteract the imperfect analog-to-digital converter (ADC) comprised in the receiver. Similar to the RT side, the power of the echo interference leakage coming from the ADC becomes lower than the noise floor power at high frequency, therefore, the zeroing technique could also be applied at the CO side.

In the future, the impact of the reduced complexity technique may be more important, especially in the case where the service providers decide to go for a coordinated system in which the transmit signals of the modems located on the central office side, and which are transmitting in the same bundle of wires, are known from all CO modems. In such a case, the CO modems could implement near-end crosstalk cancellers to eliminate the near-end crosstalk that comes from other wires in the bundle. The structure of the near-end crosstalk canceller is identical to that of the echo canceller structure [26]; only their signal source is different. In such a coordinated system, the number of required operations could become a very important issue since many near-end crosstalk cancellers (one per twisted-wire-pair in the bundle) would be required for each CO modem.

References

[1] J. M. Cioffi and J. A. C. Bingham, "A data-driven multitone echo canceller," *IEEE Trans. Commun.*, vol. 42, pp. 2853–2869, Oct. 1994.

[2] M. Ho, J. M. Cioffi, and J. A. Bingham, "Discrete multitone echo cancellation," *IEEE Trans. Commun.*, vol. 44, pp. 817–825, July 1996.

[3] D. C. Jones, "Frequency domain echo cancellation for discrete multitone asymmetric digital subscriber line transceivers," *IEEE Trans. Commun.*, vol. 43, pp. 1663–16672, Feb. 1995.

[4] M. Milosevic, T. Inoue, P. Molnar, and B. L. Evans, "Fast unbiased echo canceller update during ADSL transmission," *IEEE Trans. Commun.*, vol. 51, pp. 561–565, Apr. 2003.

[5] G. Ysebaert, K. Vanbleu, G. Cuypers, M. Moonen, and K. V. Acker, "Double talk cancellation in echo cancelled DMT-systems," in *European Signal Processing Conference*, vol. 2, pp. 381–384, Sept. 2002.

[6] G. Ysebaert, K. Vanbleu, G. Cuypers, M. Moonen, and J. Verlinden, "Echo cancellation for discrete multitone frame-asynchronous ADSL transceivers," in *IEEE International Conference on Communications*, vol. 4, pp. 2421–2425, May 2003.

[7] A. Erdogan, B. Alder, T.-H. Sang, and A. Karacas, "Efficient implementation of echo canceller for applications with asymmetric rates," *International Conference on Acoustics, Speech, and Signal Processing (ICASSP 2003)*, vol. 6, pp. 233–236, Apr. 2003.

[8] H. V. Sorensen and C. S. Burrus, "Efficient computation of the DFT with only a subset of input or output points," *IEEE Trans. Commun.*, vol. 41, pp. 1184–1200, Mar. 1993.

[9] A. Wu, T. Chan, and B. Wang, "A fast algorithm for reduced-complexity programmable DSP implementation of the IFFT/FFT in DMT systems," *IEEE Workshop on Signal Processing Systems*, pp. 356–365, Oct. 1998.

[10] J. G. Proakis and D. G. Manolakis, *Digital Signal Processing.* Prentice Hall, third ed., 1996.

[11] J. M. Cioffi, "A multicarrier primer," *ANSI T1.4 Contributions Boca Raton*, pp. 91–157, Nov. 1991.

[12] W. Y. Chen, J. L. Dixon, and D. L. Waring, "High bit rate digital subscriber line echo cancellation," *IEEE Trans. Commun.*, vol. 9, pp. 848–860, Aug. 1991.

[13] *Asymmetrical Digital Subscriber Line (ADSL) transceivers- G992.1.* International Telecommunication Union (ITU), June 1999.

[14] N. Al-Dhahir and J. M. Cioffi, "Optimum finite-length equalization for multicarrier transceivers," *IEEE Trans. Commun.*, vol. 44, pp. 56–64, Jan. 1996.

[15] W. Henkel, "An algorithm for determining the DMT time-domain equalizer coefficients," *ETSI Contribution TD26*, pp. 56–64, Sept. 1997.

[16] J. M. Cioffi and G. D. Forney, "Generalized decision-feedback equalization for packet transmission with ISI and Gaussian noise," *in Communications, Computation, Control and Signal Processing:a tribute to Thomas Kailath*, 1997.

[17] *American National Standard Draft proposed, Spectrum Management for Loop Transmission Systems, Issue 2.* Committee T1 - Telecommunication, Aug. 2002.

[18] T. Starr, J. M. Cioffi, and P. J. Silverman, *Understanding Digital Subscriber Line Technology.* Prentice Hall, 1999.

[19] *Network and Customer Installation Interfaces Asymmetric Digital Subscriber Line (ADSL) Metallic Interface.* ANSI T1.413, June 1998.

[20] T1E1.4, *Interface between networks and customer installation, Very-High-bit-rate digital subscriber lines (VDSL), metallic interface (DMT based).* Alliance for Telecommunications Industry Solutions (ATIS), June 2004.

[21] M. Isaksson, F. Sjoberg, R. Nilsson, P. Olding, D. Bengtsson, and D. Mestdagh, "Pulse shaping with zipper - Spectral compatibility and asynchrony," *T1E1.4 Technical subcomittee working group*, pp. 1–6, Mar. 1998.

[22] D. G. Manolakis, V. K. Ingle, and S. M. Kogon, *Statistical and Adaptive Signal Processing.* McGraw-Hill Higher Education, first ed., 2000.

[23] G. A. Zimmerman, "Challenges for 10 Gb/s implementation on UTP media," *CMP Media LLC*, 2005.

[24] G. Arslan, M. Ding, B. Lu, M. Milosevic, Z. Shen, and B. L. Evans, "UT Austin multicarrier equalizer design toolbox for Matlab." The University of Texas at Austin, May 2001. Software.

[25] J. Z. H. Wu and C. Lash, "Taking the noise out of adsl modem designs." Internet document, 2003. http://www.commsdesign.com/design _ corner/showArticle.jhtml?articleID=16500635.

[26] T. Starr, M. Sorbara, J. M. Cioffi, and P. J. Silverman, *DSL Advances*. Prentice Hall, 2003.